BNL-101524-2014-TECH

AD/AP 34;BNL-101524-2013-IR

Long-Term Tracking with Patris (using a RHIC test lattice) Part 1. Search of Physical and Dynamic Aperture with Sextupoles

J. Milutinovic

January 1992

Collider Accelerator Department

Brookhaven National Laboratory

U.S. Department of Energy

USDOE Office of Science (SC)

DISCLAIMER

AD/AP-34

Accelerator Development Department
Accelerator Physics Division
BROOKHAVEN NATIONAL LABORATORY
Associated Universities, Inc.
Upton, NY 11973

Accelerator Physics Technical Note No. 34

LONG-TERM TRACKING WITH PATRIS (using a RHIC test lattice) Part 1. Search of Physical and Dynamic Aperture with Sextupoles

J. Milutinovic and A.G. Ruggiero

January 1992

LONG-TERM TRACKING WITH PATRIS
(using a RHIC test lattice)
Part 1. Search of Physical and Dynamic Aperture with Sextupoles

J. Milutinovic and A.G. Ruggiero

Accelerator Development Department
Brookhaven National Laboratory
January 1992

Contents

LONG-TERM TRACKING WITH PATRIS (using a RHIC test lattice) Part 1. Search of Physical and Dynamic Aperture with Sextupoles

J. Milutinovic and A.G. Ruggiero
Accelerator Development Department
Brookhaven National Laboratory
January 1992

1. Introduction and Motivation

We are initiating a program of research to determine the stability of the motion of a single particle circulating in a storage ring for a very long period of time. The method we intend to use is to perform simulation of the motion by computer tracking; we shall perform a variety of computer experiments to subject the motion of the particle to a sequence of tests under a wide range of conditions. For this purpose we are planning to use the computer code PATRIS, a program which simulates the particle motion either by a 7×7 matrix representation wherever the motion is assumed linear in the standard variables x, x' and y, y' which represent the displacements from an ideal reference closed orbit, or by applying *kicks* at the locations where non-linear elements, like sextupoles and magnet field imperfections, are located. The non-linear elements are approximated with a zero-length extension. The PATRIS code has been described briefly in Ref. 1 and has been demonstrated[2] to have the capability to treat the motion of a particle satisfying the *symplectic* conditions; moreover it can treat closed orbit distortions exactly and provide a variety of correction schemes. Linear errors and field imperfections like magnet displacements, dipole field errors, regular and skew quadrupole errors are calculated with the 7×7 matrix representation and do not need to be taken *lumped* or as *kicks*. Also the code can simulate synchrotron oscillations due to presence of rf cavities in the most accurate fashion. This code is available and runs on the CRAY, at Livermore National Laboratory.

We have adopted the Relativistic Heavy Ion Collider (RHIC) as the test bench for our computer experiments and investigation. The lattice used for this collider is close to the one being proposed, but at the same time simplified to reduce the amount of bookkeeping. The basic features are included. Moreover we do not expect that the results of our research will depend so crucially on the very fine details. The particle the motion of which is being investigated is a heavy particle, like a proton or a heavy ion, completely stripped of electrons, for instance Au. It is assumed that these particles do not lose energy by radiation and thus represent pure conservative systems.

During our computer-experimental program we shall investigate the effects of magnet imperfections and other related issues. We shall proceed in stages by successive iteration, from a simpler to a more complicated or inclusive model. At the same time we shall always check the validity of our results which, after all, are obtained with the help of a computer. We shall thus perform test of reversibility or repeatability, and check the effects of the computer precision, accuracy and the propagation of the round-off errors. As results are gathered and a particular issue satisfactorily examined to a point of conclusion, the information will be reported in a formal technical note. This represents the first of such reports.

This technical note describes to some details the *test lattice* we have adopted for our program of research in Section 2. The basic performance of the lattice adopted and comparison of the results obtained with three major codes are explained in Section 3. A discussion of the physical betatron acceptance of the collider in absence of any type of imperfections and of the main sextupole magnets is then given in Section 4. Finally the effect of the main sextupoles on the physical and dynamic aperture is discussed in Sections 5 and 6.

2. The Test Lattice

In order to carry out our program of research on the long-term stability of the particle motion, we have used the lattice of the storage ring described in Ref. 3, which goes under the name of RHICAGR. Such a lattice has been proposed as a possible solution for the RHIC,[4] has already several features adopted for this project, and closely resembles the one that will ultimately be built. For the type of study we are planning, we do not believe that the final details of the storage ring lattice are very relevant: our interest is in determining the basic features of the stability of the particle motion; thus, in our opinion the adoption of the RHICAGR as the test lattice is an adequate choice. The structure is simplified and reduce the burden of bookkeeping on the computer. The motivations for this lattice can be found in Ref. 3. We give below a summary of the relevant features so that the reader can easily reconstruct the outline and shape of the storage ring.

The major parameters of RHICAGR are given in Table 1. The lattice has a threefold periodicity. Each superperiod has the following sequential structure:

.ARO .OI1 .OI2 .ARI .IO1 .IO2

The beam moves in the anticlockwise direction and we have chosen the beginning of the outer arc as the start of the superperiod. The modules in the sequence are as follows:

.ARO the outer arc, made of 12 regular FODO cells,

.OI1 the first part of the insertion that takes the beam from the outer arc to the first crossing point,

.OI2 the second part of the insertion that takes the beam from the first crossing point to the beginning of the inner arc,

.ARI the inner arc, also made of 12 regular FODO cells,

.IO1 the first part of the insertion that takes the beam from the inner arc to the second crossing point,

.IO2 the second part of the insertion that takes the beam from the second crossing point to the outer arc.

Sextupoles are located only in the arcs and, for simplicity, are lumped in the middle of the regular arc quadrupoles. There are no sextupoles in the insertions. The only other elements involved in the lattice description are drifts, dipoles and quadrupoles. The outer

and inner arcs .ARO and .ARI have the same structure, that is:

$$3(.C1 \quad .C2) \qquad 3(.C2 \quad .C1)$$

where

$$.C1 = \begin{array}{cccccc} SD1 & QD/2 & O & B & O & QF/2 \\ SF1 & QF/2 & O & B & O & QD/2 \end{array}$$

and .C2 has the same structure except that the sextupoles SD1 and SF1 are replaced respectively by the sextupoles SD2 and SF2. The drift O is 2.12393 m in the outer arc and 2.10712 m in the inner arc. Also the strength of the sextupoles is different in the inner and outer arcs according to the values of Table 2. There are a total of 8 sextupole families with a distribution that reflects the threefold superperiodicity of the ring.

Table 1: General Parameters

Circumference	3833.8450 m
Average Radius	610.1754 m
Bending Radius	253.1137 m
Periodicity	3
Betatron Tunes: Hor.	34.82489
Ver.	28.82433
Transition Energy	24.76
Natural Chromaticity: Hor.	−104.25
Ver.	−78.47
Beta* (in all crossing points)	2.0 m
Crossing Angle	0. mrad (head-on)

Table 2: The Sextupole Families

($B''\ell/B\rho$ in m^{-2})

	Inner Arc (.ARI)	Outer Arc (.ARO)
SD1	−0.41793	−0.56172
SD2	0.10850	−0.96243
SF1	0.11051	0.34953
SF2	0.06656	0.55521

Each arc and each insertion begin and end in the middle of regular QD quadrupoles. The structure of each insertion is made of a dispersion killer section followed by a five-quadrupole telescope for beta-tuning. Intermixed with the telescope quadrupoles, there are special dipoles which bring the two beams in collision by moving each beam from the outer to the inner side and vice versa. The structure for the first part of the first insertion is

.OI1 = QD/2	O2	B2	L2	QF	L1	B2
	O1	QDK	LE	QF	O	B
	O	O7	Q5	O6S	O6L	Q4
	O5	BC3	O4	Q3	O3	Q2
	O2	Q1	O1L	O1S	BC2	LCS
	LCL	BC1	LO			

The structure of the second pair of the same insertion (.OI2) is obtained by mirror reflection of the first part, that is from LO back to QD/2, and by replacing the dipoles BC1, BC2 and BC3 with BD1, BD2 and BD3 respectively. The structure of the first part of the second insertion (.IO1) is similar to that of .OI1 with the exception of replacing the dipoles BC1, BC2 and BC3 with BU1, BD2 and BD3 respectively. Finally the structure of the last section (.IO2) is obtained by mirror reflection of .IO1 and by replacing the dipoles BU1, BD2 and BD3 respectively with BT1, BC2 and BC3.

The drifts in proximity of the dipoles have different lengths on the inner and outer side of the ring; their values are displayed in Table 3. All the regular dipoles B and B2 and all the quadrupoles have the same parameters wherever they appear; that is, there is no

distinction on their location, between inner and outer arcs. The insertion dipoles, on the other end, have somewhat different parameters. Table 4 gives the summary for the dipole magnets and Table 5 that for the quadrupoles.

Table 3: The Drifts. Lengths in meter.

	Outer Side	Inner Side	Bore Radius mm
O	2.12393	2.10712	36.
O1	5.69671	5.68810	36.
O2	7.21194	7.20333	36.
L1	2.99295	2.98434	36.
L2	1.63772	1.62911	36.
LE	13.52105		36.
O1S	0.6545		36.
O1L	0.6545		63.
O2	1.78860		63.
O3	4.1423		63.
O4	5.30915		63.
O5	14.77448		63.
O6S	2.0		36.
O6L	12.68438		63.
O7	7.24785		36.
LCS	3.5		36.
LCL	3.5		63.
LO	9.8		81.

Table 4: Dipole Magnets

	Length	Bend. Angle	Entr. Angle	Exit Angle
	m	mrad	mrad	mrad
B	9.45	37.335	0.0	0.0
B2	4.84	19.122	0.0	0.0
BC1	3.7	−18.836	−18.836	0.0
BC2	1.36217	5.382	0.0	0.0
BC3	3.40542	13.454	0.0	0.0
BD1	3.7	18.836	0.0	18.836
BD2	1.36217	−5.382	0.0	0.0
BD3	3.40542	−13.454	0.0	0.0
BU1	3.7	18.836	18.836	0.0
BT1	3.7	−18.836	0.0	−18.836

Table 5: Quadrupole Magnets

	Length	$B'/B\rho$	Bore Radius
	m	m^{-2}	mm
QF	1.13	0.085932	36.
QD	1.13	−0.088886	36.
QDK	1.45	−0.069270	63.
Q1	1.45	−0.066160	63.
Q2	2.25	0.086081	63.
Q3	1.45	−0.075763	63.
Q4	2.25	0.060508	63.
Q5	1.13	−0.052941	36.

In order to determine the physical and dynamic aperture of the ring, we have specified the internal dimension of the vacuum chamber; assuring that this has a circular shape, the radius is given in Table 3 for all the drifts and in Table 5 for all the quadrupoles. The vacuum chamber inner radius for the dipoles is given in Table 6.

Table 6: Vacuum Chamber Radius in the Dipoles

B	36. mm
B2	36.
BC1	81.
BC2	36.
BC3	63.
BD1	81.
BD2	36.
BD3	63.
BU1	81.
BT1	81.

All the sextupoles in the arcs have also been taken with the reference vacuum chamber radius of 36. mm.

3. Basic Performance of RHICAGR

The most fundamental parameters of the test lattice are shown in Table 1. The parameters are set for tuning all six crossing regions to the same value of $\beta^* = 2$ m. To be observed that the insertions have a symmetric quadrupole arrangement.* The uncorrected (natural) chromaticity is also shown in Table 1; the sextupoles are set to the values shown in Table 2 in order to cancel the chromaticity exactly at the center of the momentum aperture and to flatten the dependence of the tunes with momentum errors over a range of $\pm 0.5\%$. The sextupole adjustment has been calculated with the code MAD.

The amplitude lattice functions, horizontal and vertical, are plotted in Fig. 1; the behavior of the horizontal dispersion is shown in Fig. 2. The calculations have been done with the SYNCH program. To be noticed that the dispersion is zero at the crossing point; but there is a finite derivative which makes the dispersion change sign between the two sides of the crossing point. The dispersion is effectively zero between the last regular dipole (B) and the first dipole for beam crossing (that is BC3, for instance). The maximum value of beta is 630 m which occurs in the middle of Q3. In the arcs the maximum value of beta is 50 m; the maximum value of the dispersion is 1.57 m.

The lattice functions have been calculated using three different codes: SYNCH,[5] MAD,[6] and PATRIS.[1] There is remarkable agreement among the results obtained from these codes, to several significant digits as it can be seen from Table 7. The chromatic properties of the lattice, that is the dependence of some of the lattice functions on the momentum error δ, are displayed in Figs. 3 to 8 over the momentum range of interest for RHIC of $\pm 0.6\%$. The variation of both betatron tunes is given in Fig. 3; it is seen that there is some discrepancy among the three codes, with SYNCH providing results larger and MAD smaller when compared to those from PATRIS. The results from PATRIS are given by the continuous line, since for us they represent the reference case; the results from MAD are filled circles and those from SYNCH crosses. The discrepancy of the results increases with the momentum error: at the extreme end of $\pm 0.6\%$ the error in tune is as large as 0.008.

* The actual lattice for RHIC will have eventually an anti-symmetric arrangement.

Figures 4 and 5 plot the variation of the lattice functions, horizontal beta and dispersion in the middle of the centermost QF, and the vertical beta in the middle of the centermost QD in the outer arc. It is seen that whereas there is in general very good agreement among all the codes, there is a substantial difference of the dispersion behavior as calculated from PATRIS from that obtained from the other two codes. This is seen also in Fig. 7 which plots the dispersion function at the location of the first crossing of the superperiod. On the other hand, there is a very good agreement among all the three codes for the estimates of the beta functions as shown in Fig. 6 which displays the behavior of the amplitude functions at the location of the first crossing, and in Fig. 8 which plots the maximum value of the amplitude functions encountered either in the middle of Q2 or in the middle of Q3.

Table 7: Comparison of Lattice Functions Among Three Codes

	SYNCH	MAD	PATRIS
Q-Hor.	34.82489	34.82489	34.82489
Q-Ver.	28.82433	28.82433	28.82433
γ_t	24.76053	24.88267	24.65527
Chrom.-Hor.	−104.24718	−104.2518	−104.39702
Chrom.-Ver.	−78.47364	−78.47512	−78.54927
Beta*-Hor.	2.00491	2.005	2.00491
Beta*-Ver.	2.00141	2.001	2.00141
Beta-Hor.@QF	50.69886	50.699	50.69886
Beta-Ver.@QD	50.02812	50.028	50.02814
Beta-Hor.max	587.98930	587.989286	587.98929
Beta-Ver.max	629.60603	629.605953	629.60595
Disper.@QF	1.57125	1.571	1.57125
Dispersion*	0.00024	0.000	0.00024

Beta and Dispersion in meter. Chromaticities are natural.

4. The Physical Betatron Acceptance

In principle the magnet aperture should be chosen to avoid limitations on the physical acceptance around the ring. A summary of the effects of the magnet aperture is shown in Table 8. For each magnet we list the maximum beta-value; in parenthesis whether the maximum occurs in the horizontal (H) or vertical (V) plane or in both; the vacuum chamber radius; and the acceptance defined as

$$Acceptance = (radius)^2 / \beta \tag{1}$$

The betatron acceptance in the arcs does not change with β^* and should be taken as the reference. There is a limitation to 6 πmm·mrad at Q2 and Q3. There is a bottleneck in BC2 which yields to an acceptance of 5.4 πmm·mrad.

Table 8: Absolute Physical Betatron Acceptance

Magnet	Beta	Radius	Acceptance
QF (H)	50.7 m	36 mm	25.6 πmm·mrad
QD (V)	50.1	36	25.9
Q1 (H)	297.	63	13.4
Q2 (H)	588.	63	6.7
Q3 (V)	630.	63	6.3
Q4 (H)	103.	63	38.5
Q5 (V)	93.	36	13.9
BC1 (H&V)	93.	81	70.0
BC2 (H&V)	241.	36	5.4
BC3 (V)	384.	63	9.7

The PATRIS code makes a scan throughout the ring structure searching for the limitations on the betatron acceptance of both the horizontal and vertical plane; the search is based on the actual physical aperture set in input and the calculated amplitude lattice functions for the ideal lattice and for a particle with no momentum error ($\delta = 0$). The result from

PATRIS is that there is indeed a bottleneck in correspondence of the end of the BC2 dipole where β is larger for both planes, and the betatron acceptance being limited there is 5.08 πmm·mrad in agreement with the value shown in Table 8. The full beam emittance in the RHIC can be, but will not exceed in any circumstance, 1 πmm·mrad; thus there is a safety factor of at least 5 between the betatron acceptance of the collider and the full beam emittance; this of course is true in absence of any error.

We have also determined the betatron acceptance of RHIC by tracking with PATRIS. We have adopted the following procedure:

- We set the off-momentum value δ of the particle to be tracked to a value in the range of $\pm 0.6\%$. The particle motion is launched in the middle of the QD quadrupole at the beginning of the superperiod as specified above, that is at the beginning of the outer arc .ARO. At this point all the relevant lattice parameters are calculated for the off-momentum value δ. The sextupoles are turned off and the lattice parameters versus δ are plotted for this case in Figs. 10 to 12 (obtained with PATRIS) at the location of those elements in proximity of the determined aperture bottleneck.
- We set the initial conditions of the particle by choosing first its amplitude of motion by specifying the invariant emittances ϵ_h and ϵ_v for the horizontal and vertical plane respectively. The actual coordinates for the betatron motion are then calculated by letting $x' = y' = 0$ always, and estimating the actual horizontal x and vertical displacement y from the calculated lattice functions and the amplitude values according to the formula

$$\epsilon_{h,v}/\pi = (\gamma)_{h,v}\,(x, y)^2 \tag{2}$$

  The coordinates of the center of oscillation due to the off-momentum value are then added to the initial values of the betatron motion to obtain the total initial coordinates.
- Eight different cases are considered, depending on the relative choice of the initial horizontal and vertical betatron amplitudes; these are specified according to Table 9 below.

Table 9: Cases of Betatron Emittance Scanning

Case#	ϵ_h & ϵ_v	β-coordinates
1	$\epsilon_v = 0$	x-init.>0
2	$\epsilon_v = \epsilon_h$	x-init.>0; y-init.>0
3	$\epsilon_h = 0$	y-init.>0
4	$\epsilon_v = \epsilon_h$	x-init.<0; y-init.>0
5	$\epsilon_v = 0$	x-init.<0
6	$\epsilon_v = \epsilon_h$	x-init.<0; y-init.<0
7	$\epsilon_h = 0$	y-init.<0
8	$\epsilon_v = \epsilon_h$	x-init.>0; y-init.<0

These cases are better described in Fig. 9 which shows the betatron phase space in a two-dimensional representation with ϵ_h on the horizontal ϵ_v on the vertical axis respectively. The positive side of each axis would then represent positive values for the betatron initial displacement; whereas the negative side would correspond to negative initial values. That is the aperture scanning is done with tracking by choosing particle initial conditions moving along each of the eight lines shown in Fig. 9, corresponding to the cases of Table 9.

- The betatron acceptance limitation is searched by increasing the amplitude of the betatron motion in small steps, not exceeding 0.1 πmm·mrad. A particle is tracked for at least 1000 revolutions and its position is checked with respect to the physical aperture set at the location of the bottlenecks found by PATRIS analytically. Once any of the particle coordinates exceeds the physical aperture, the particle is considered lost and the betatron acceptance with the corresponding location recorded.

The results are shown in Fig. 13 which gives the area of stability over 1000 revolutions. There is a pure fourfold symmetry; inspection of the first quadrant is sufficient to understand the behavior of the betatron acceptance. The squarish shape is due to our way of setting the physical aperture of the various elements: in our model the vacuum chamber

has indeed the shape of a square. The same results are plotted also in Fig. 14 versus δ only for cases 1 to 3 since of the involved symmetry. There is a dip in correspondence of $\delta = 0.4\%$ which can be explained with the lattice behavior shown in Figs. 10 to 12. On the horizontal plane, the betatron acceptance is reduced by a factor of two at about $\delta = -0.5\%$. The betatron acceptance determined by tracking is very well in agreement with the analytical expectations.

5. The Effects of the Sextupoles

The betatron acceptance of the test RHIC lattice has been explored by tracking with PATRIS also with the sextupole magnets on, set to the values as specified in Table 2. We have followed the same procedure described in the previous section. The results are shown in Fig. 15 which shows the area of stability after 1000 turns. There is now an up-down symmetry only; the right-left symmetry has disappeared; this is due to the large asymmetric behavior of the lattice functions at the location of the aperture bottleneck for positive and negative values of the momentum error δ, which can be seen in Fig. 17 to 19 (also obtained with PATRIS). The physical acceptance in the presence of sextupoles is also shown in Fig. 16 only for cases 1 to 5. Comparison of Figs. 13 and 14 with Figs. 15 and 16 shows clearly a significant reduction of the betatron acceptance when the sextupoles are turned on. To obtain a more direct comparison, we have shown in the center of both diagrams of Figs. 13 and 15 the area occupied by a *square* beam with a total betatron emittance of 1 πmm·mrad in both planes.

We have also determined, the same manner, the *dynamic* aperture of the lattice with sextupole magnets turned on. For this purpose we have set the physical aperture of the vacuum chamber of all the ring elements involved to 1000 mm, that is to a value so large that when a particle reaches that amplitude it can be assumed to be lost, driven away from an instability. To check if a particle is lost, during this run, we read its position at locations corresponding to the middle of every quadrupole magnet. The results are displayed in Figs. 20 and 21. They also exhibit an up-down symmetry alone; their general behavior is similar to that found for the physical acceptance with sextupoles on, as shown in Fig. 15, which can certainly be correlated to the behavior of the common lattice functions with the momentum error δ. Nevertheless, it is easily observed that the *dynamic* aperture is somewhat wider than the physical acceptance shown in Fig. 15. One is then led to conclude that by widening the vacuum chamber of elements like BC2, Q2 and Q3 it is possible to increase the actual physical betatron acceptance and recover the *dynamic* one.

Inspection of Figs. 15 and 20 shows also very clearly a reduced acceptance along the diagonals, that is cases 2, 4, 6 and 8 with respect to the normal cases along the ϵ_h and ϵ_v axis.

6. Circular Geometry

In the previous sections we have described the physical and dynamic aperture assuming a square vacuum chamber. In reality the vacuum chamber in RHIC is of circular cross-section and there are some questions about the actual shape of the beam itself. We have then repeated the same calculations to determine the acceptance limitations in the collider ring but imposing this time as criterion for the particle loss the following condition

$$x^2 + y^2 > a^2 \tag{3}$$

where x and y are the actual particle displacements respectively horizontal and vertical, and a is the inner radius of the vacuum chamber. All the other conditions to determine the acceptance values were set as already explained before. The results are shown in Figs. 22 to 24. The circle at the center of the axis represents the beam with a circular shape and a betatron emittance of 1 πmm·mrad. It is seen that the dynamic aperture is considerably larger than the physical one and that therefore there is room for improvement by widening the bore of the magnets in proximity of the acceptance restriction. Moreover there is a remarkable difference in the results for positive and negative values of the initial conditions in the horizontal plane; this is partially due to the variation of the lattice functions with the momentum error δ, and partially to the way the total initial conditions are derived by adding algebraically the contributions from the pure betatron oscillation and from the off-momentum closed orbit according to the relations

$$\begin{aligned} x_{tot} &= \pm\sqrt{\epsilon_h/\gamma_h\,(\delta)\,\pi} + X_p\,(\delta)\,\delta \\ y_{tot} &= \pm\sqrt{\epsilon_v/\gamma_v\,(\delta)\,\pi} \end{aligned} \tag{4}$$

Because of the absence of the dispersion on the vertical plane, there is always at least an up-down symmetry. Finally a comparison of Figs. 20 and 24 shows clearly a reduction of the dynamic aperture in the circular geometry case; indeed the loss criterion given by Eq. (3) is more stringent.

7. References

1. J. Milutinovic, A.G. Ruggiero, "Comparison of Accelerator Codes for a RHIC Lattice", AD/AD/TN-9, BNL, 1988.
2. E. Forest, private communication, 1988.
3. A.G. Ruggiero, "RHICAGR. A most simplified RHIC lattice", AD/AP-26, BNL, August 1991.
4. Conceptual Design of the Relativistic Heavy Ion Collider (RHIC), BNL 52195, May 1989.
5. A.A. Garren, et al., "A User's Guide to SYNCH", FN-420, Fermilab, June 1985.
6. H. Grote, F.C. Iselin, "The MAD Program, Ver. 8.4", CERN/SL/90-13 (AP) (Rev. 2).

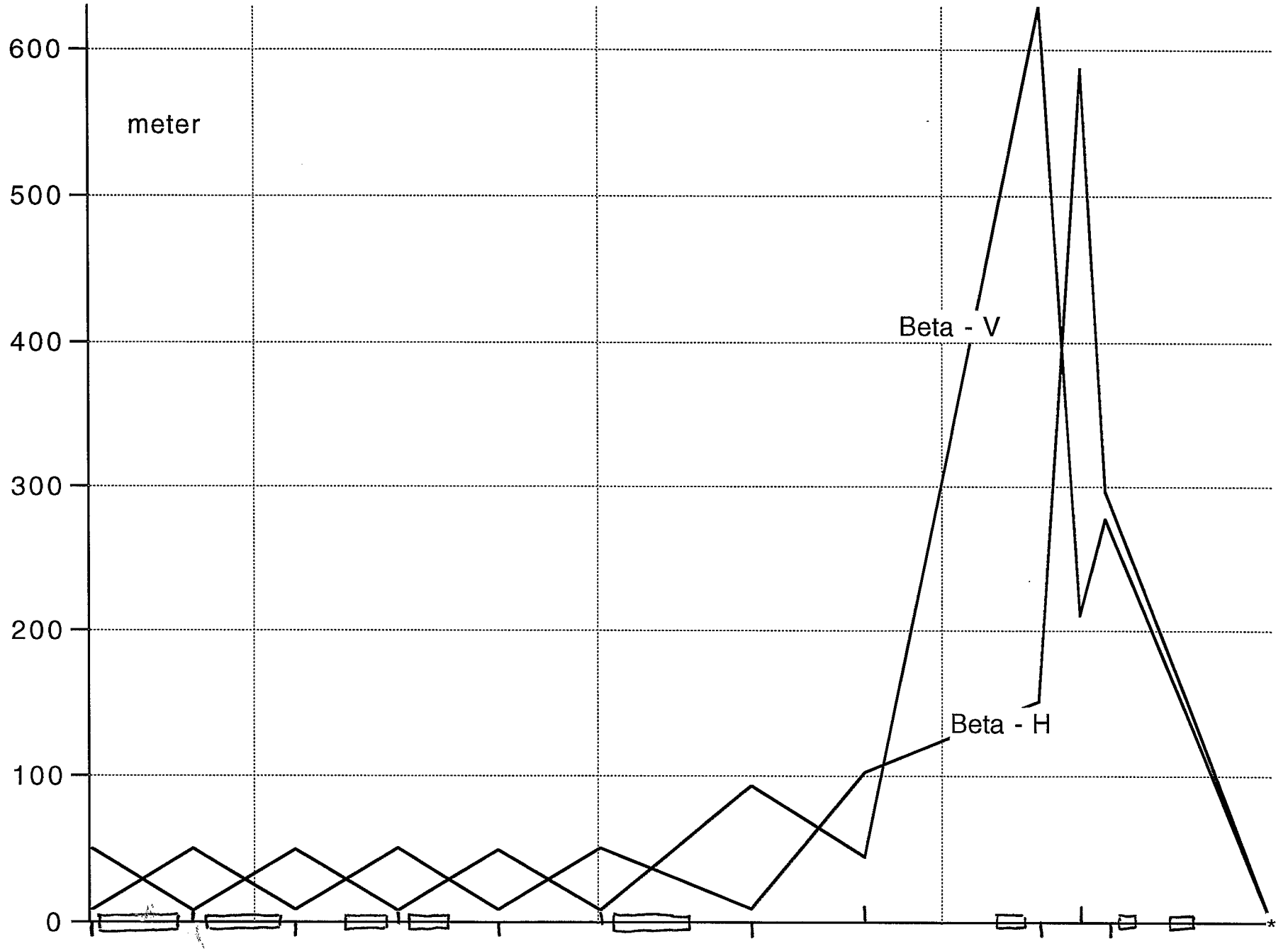

Fig. 1 The Beta - functions in RHICAGR

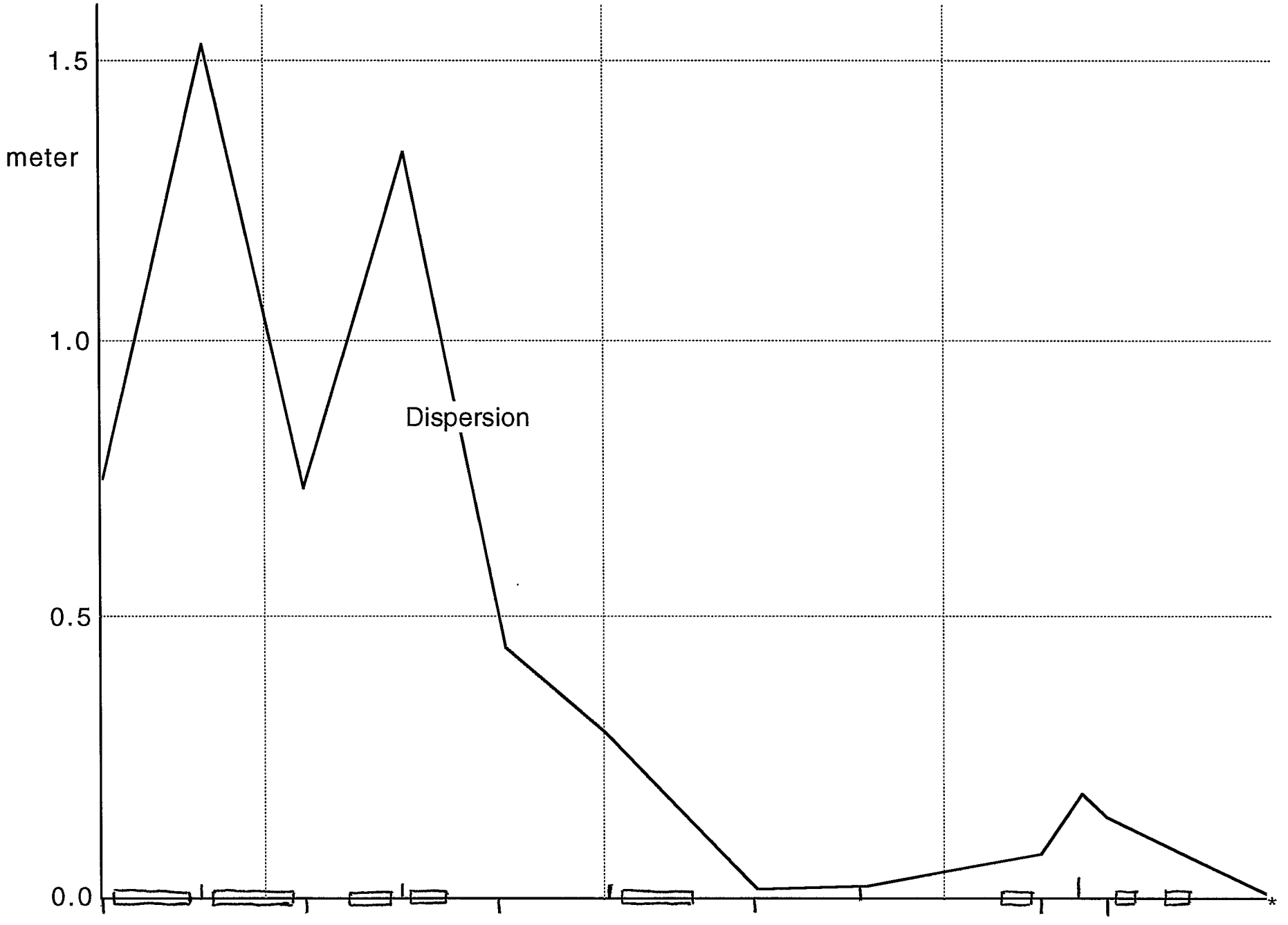

Fig. 2 The dispersion in RHICAGR

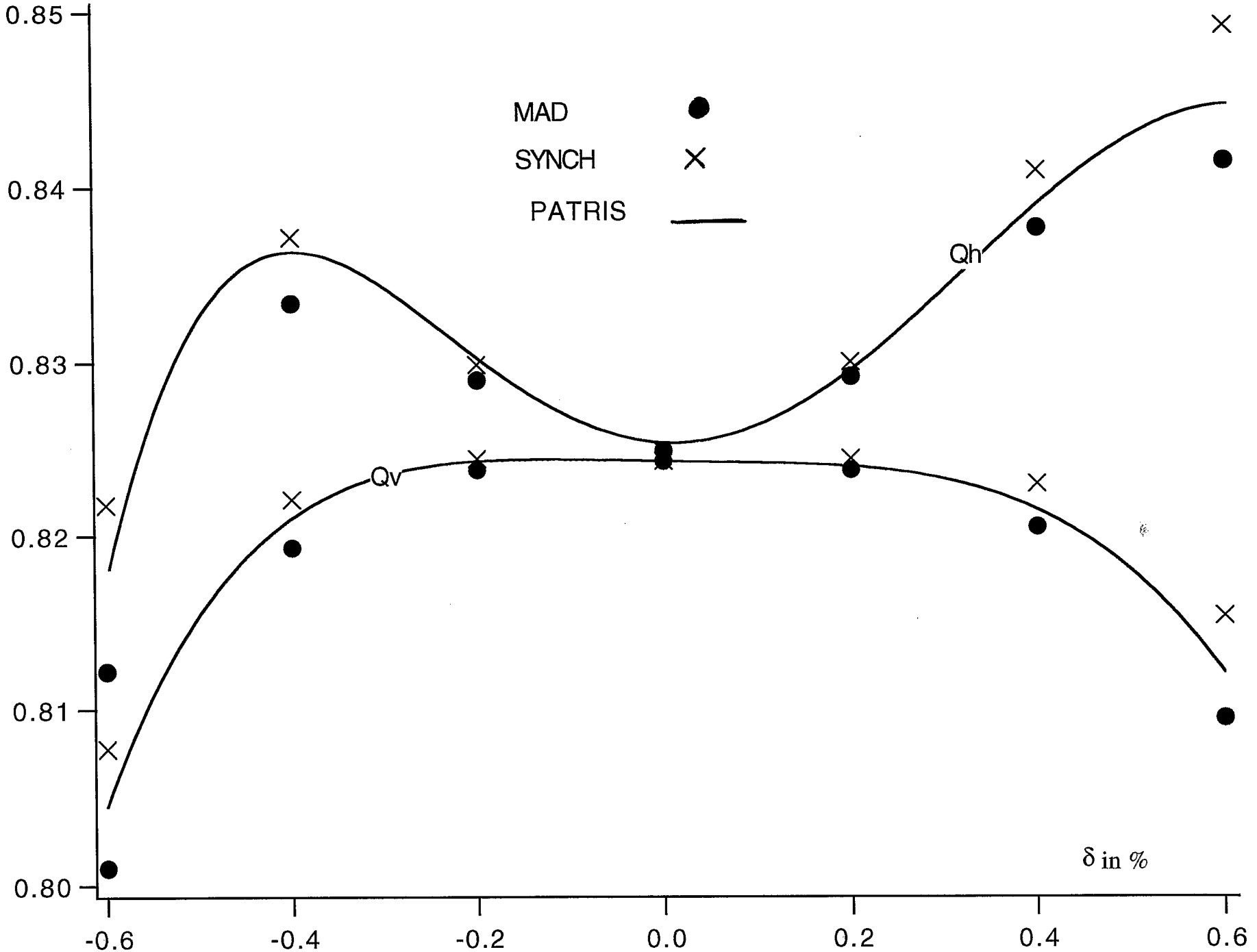

Fig. 3 Fractional Betatron Tunes vs. Momentum Error δ

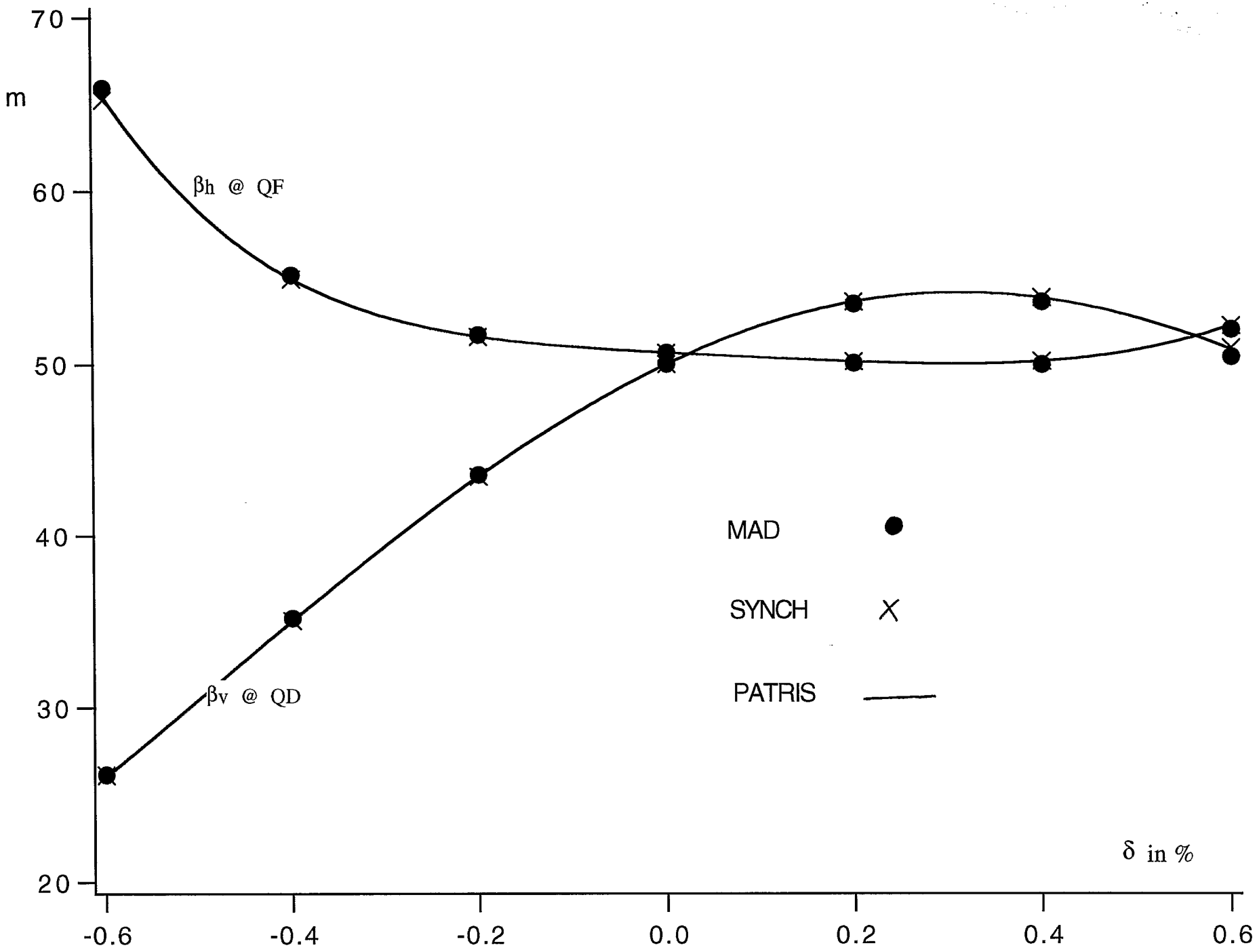

Fig. 4 Beta Functions in the Arc vs. Momentum Error δ

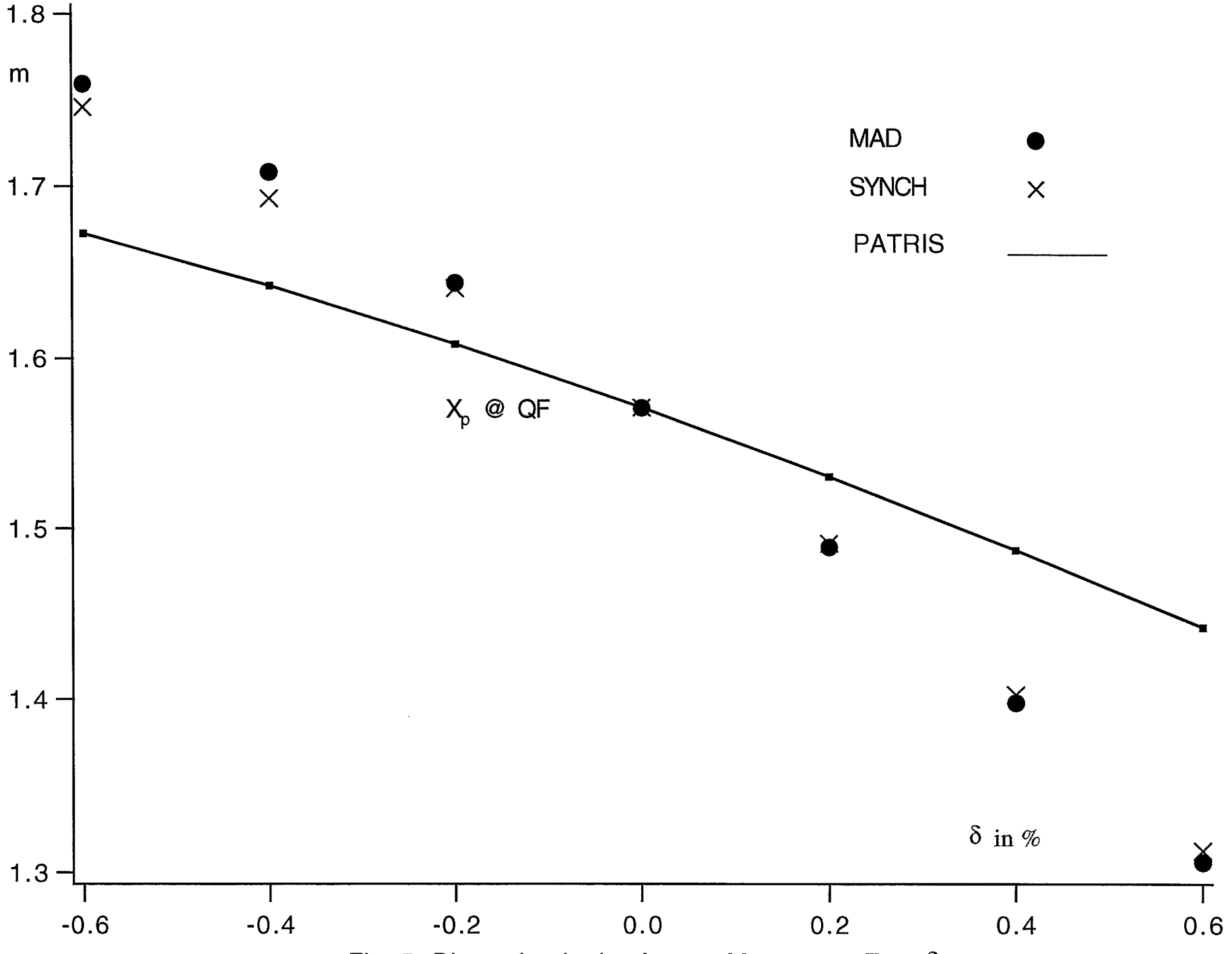

Fig. 5 Dispersion in the Arc vs. Momentum Error δ

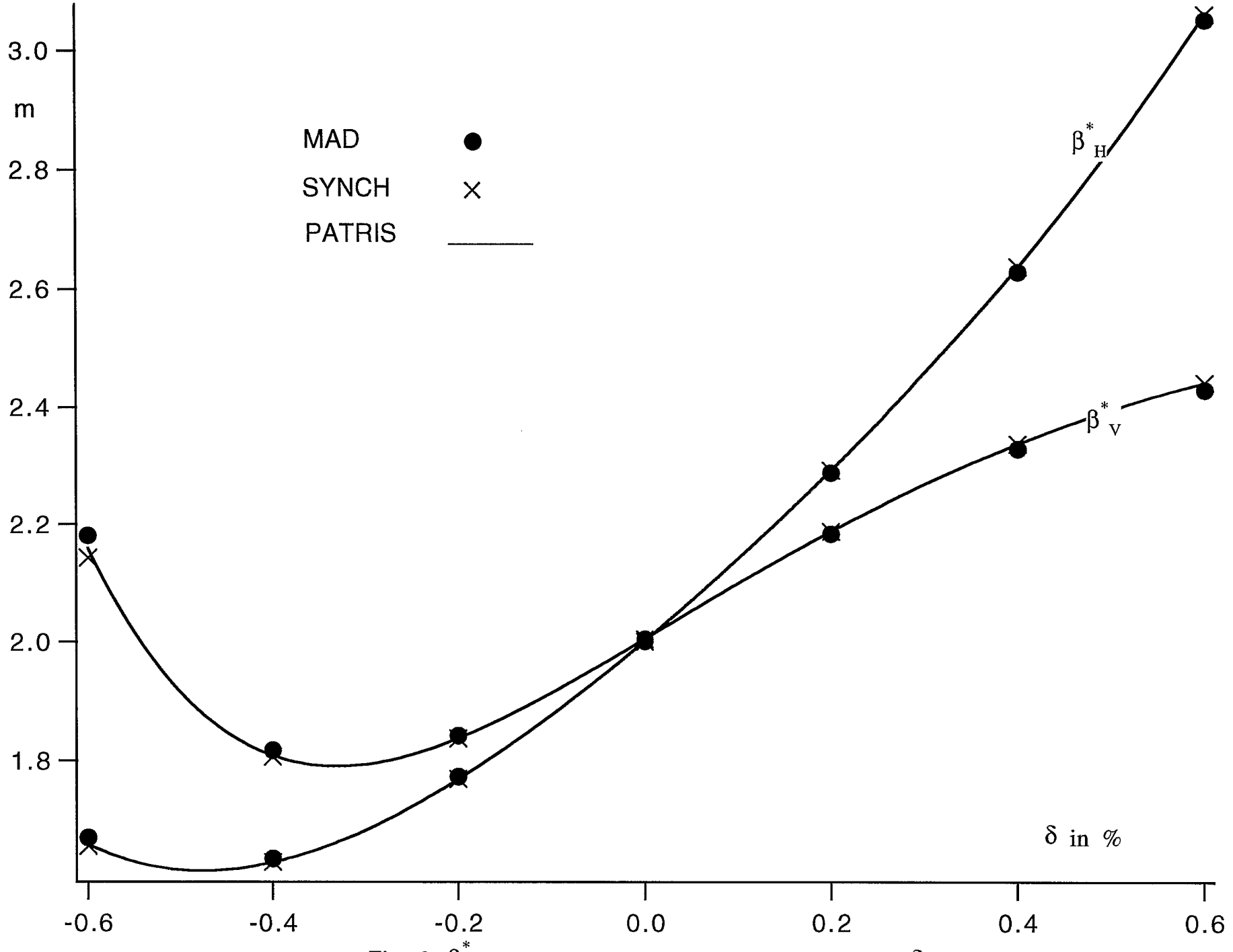

Fig. 6 β^* at first crossing point vs. momentum error δ

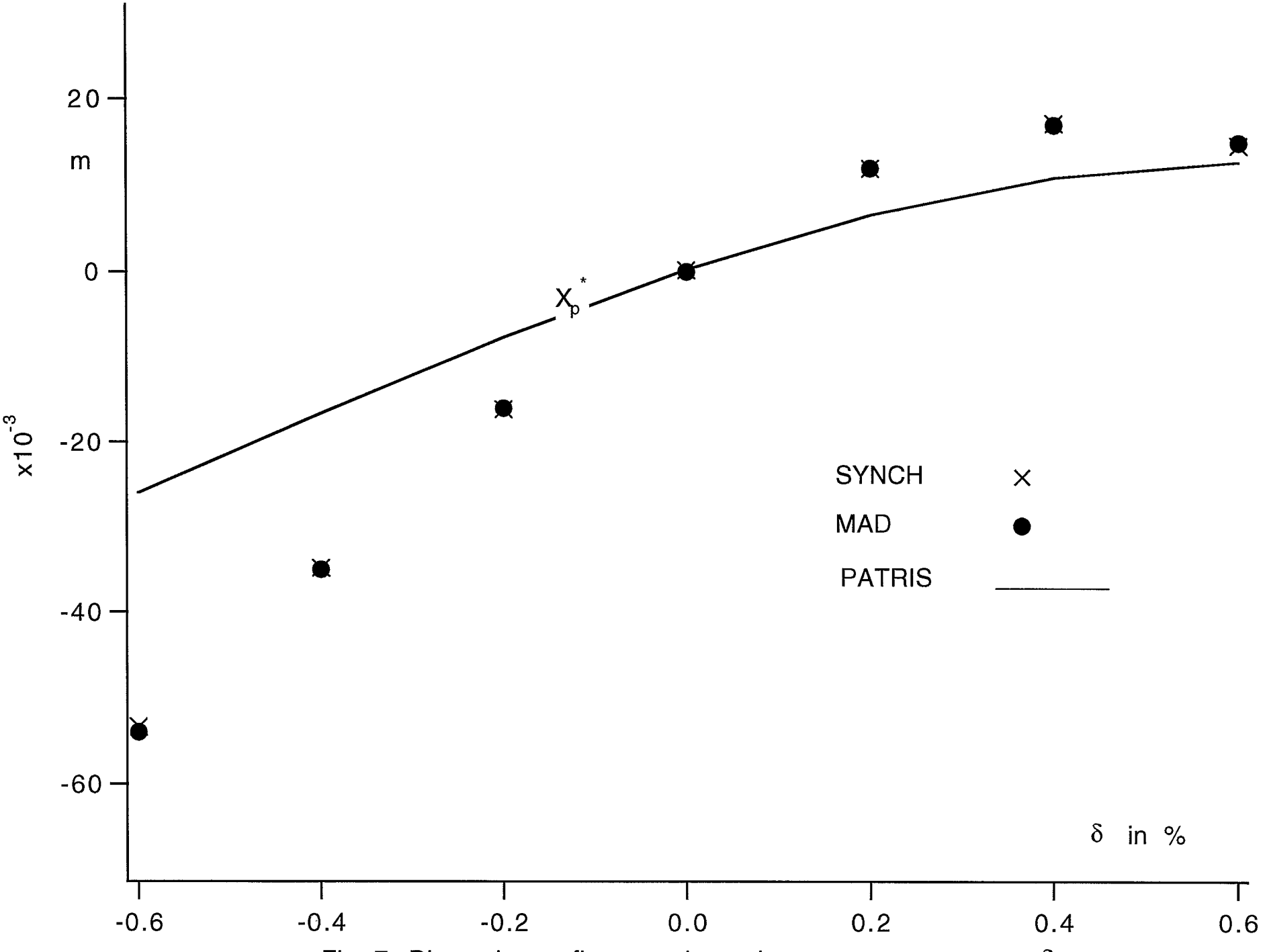

Fig. 7 Dispersion at first crossing point vs. momentum error δ

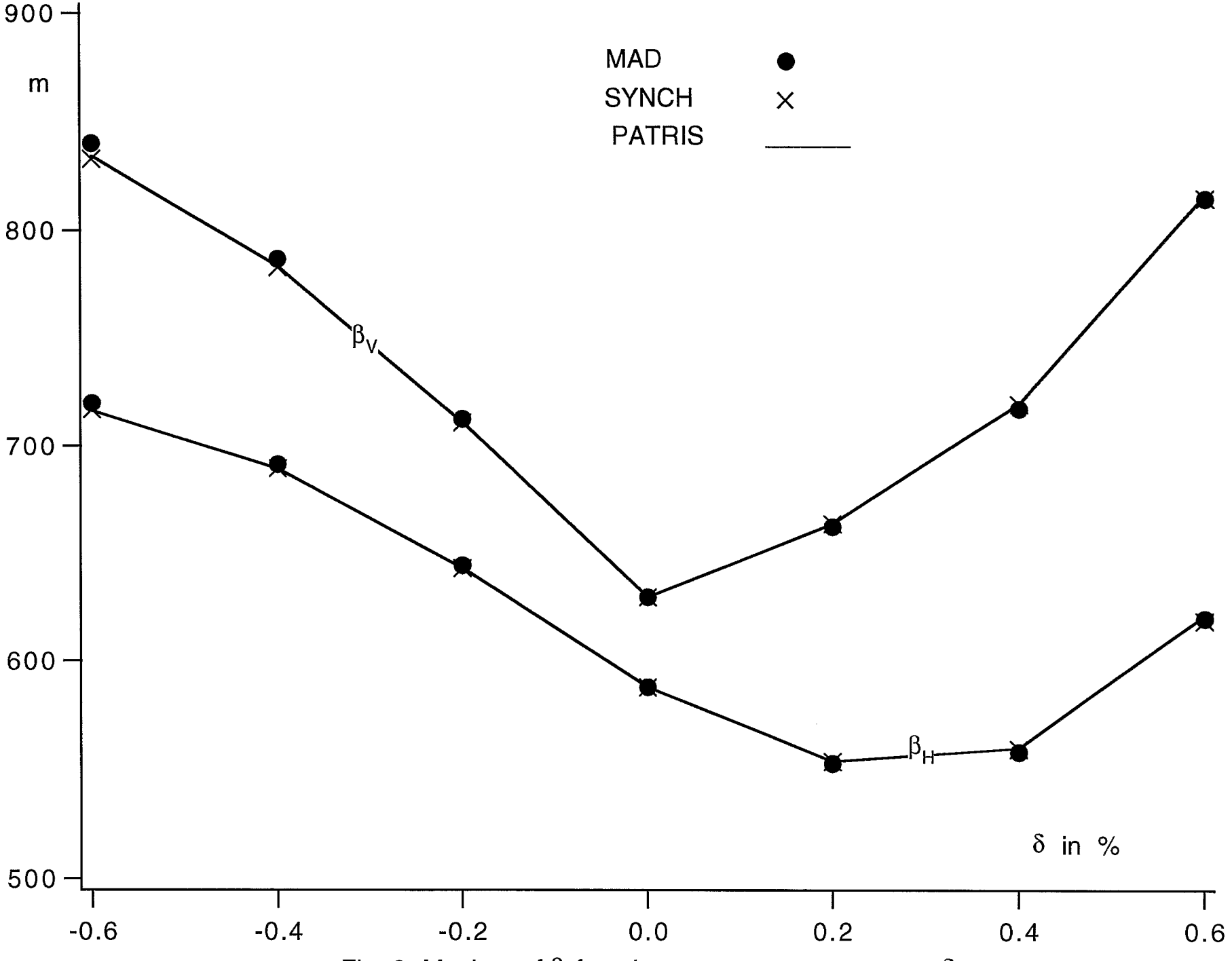

Fig. 8 Maxima of β functions vs. momentum error δ

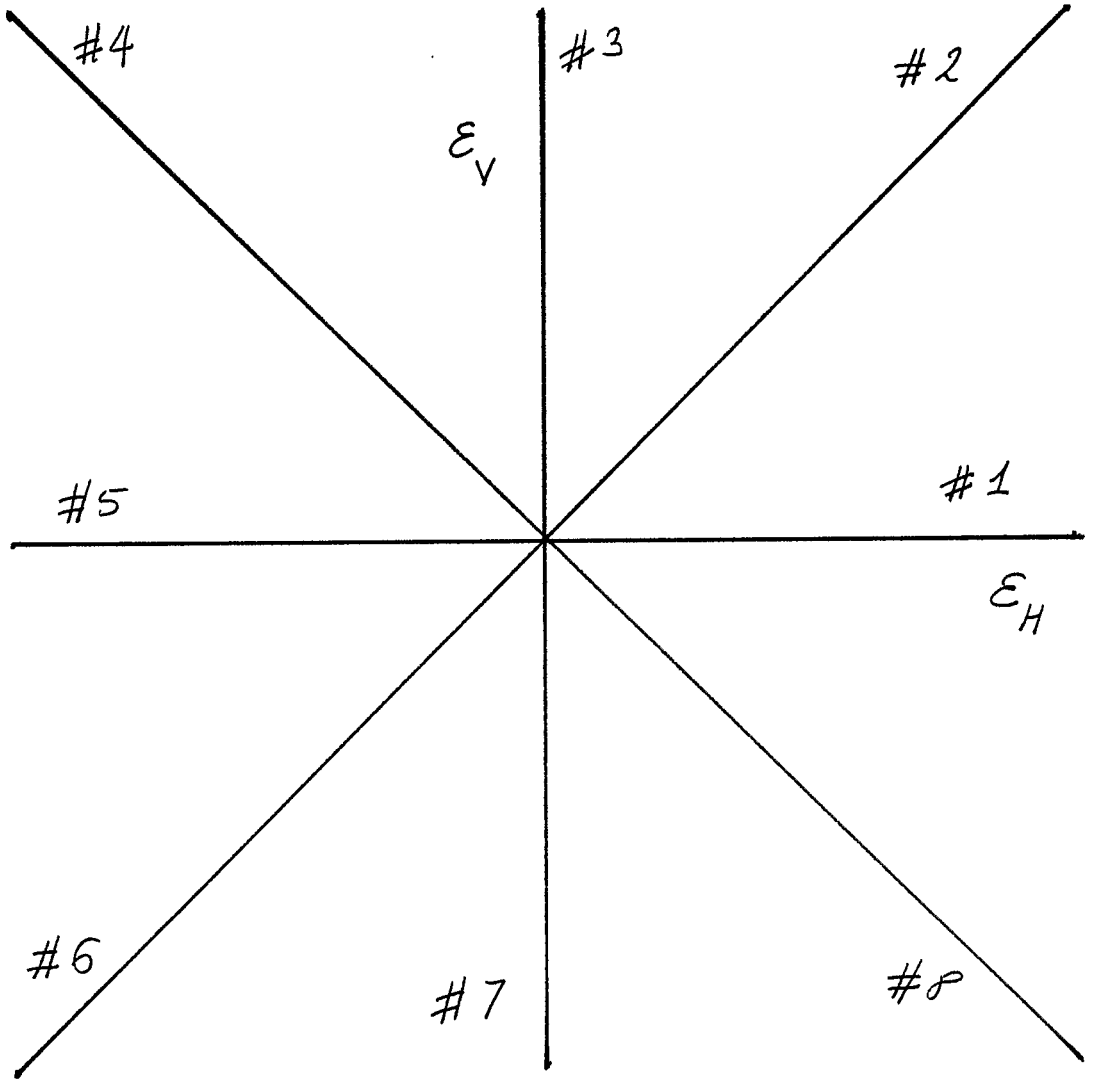

Fig. 9: Betatron Phase Space Scanning Modes

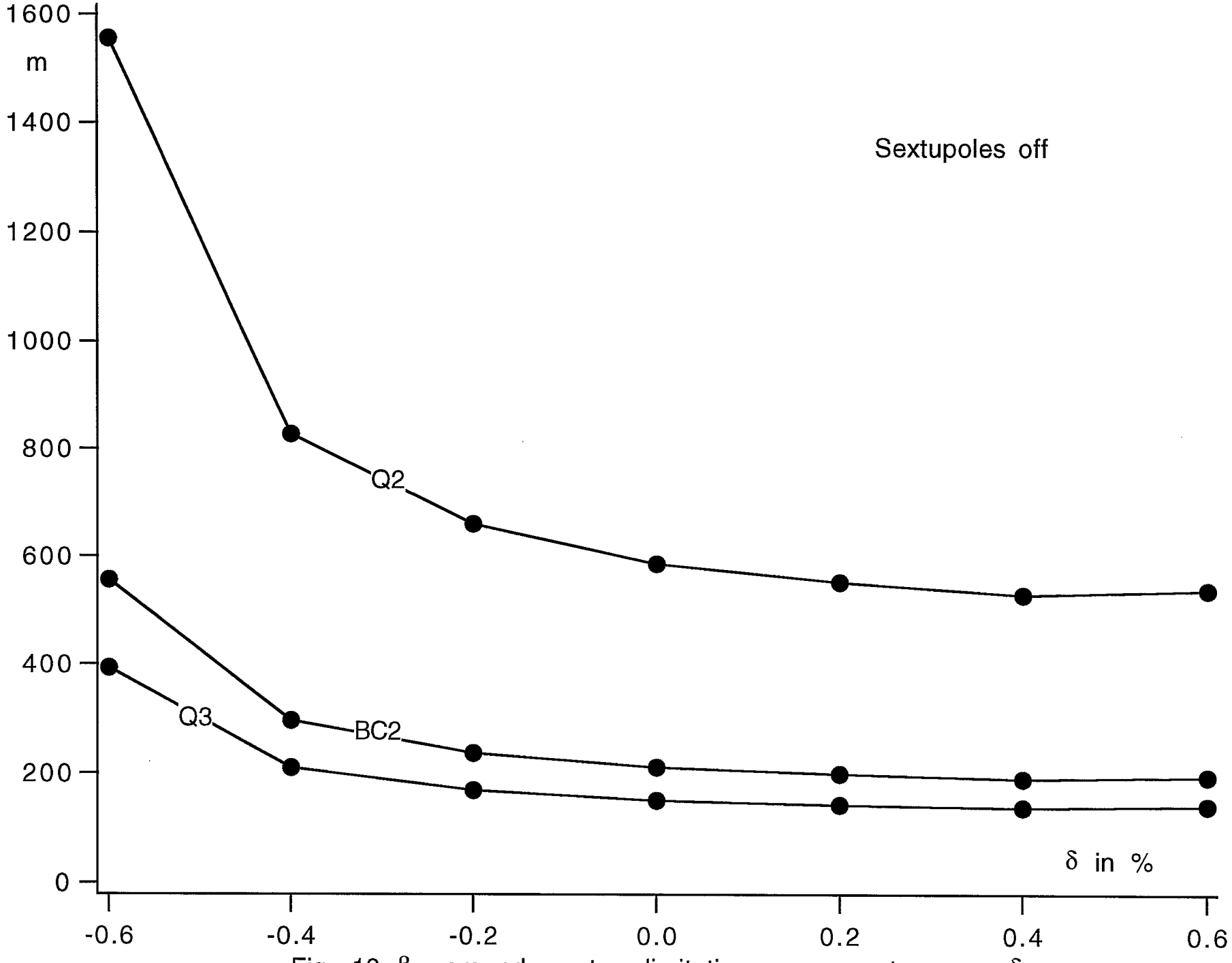

Fig. 10 β_H around aperture limitation vs. momentum error δ

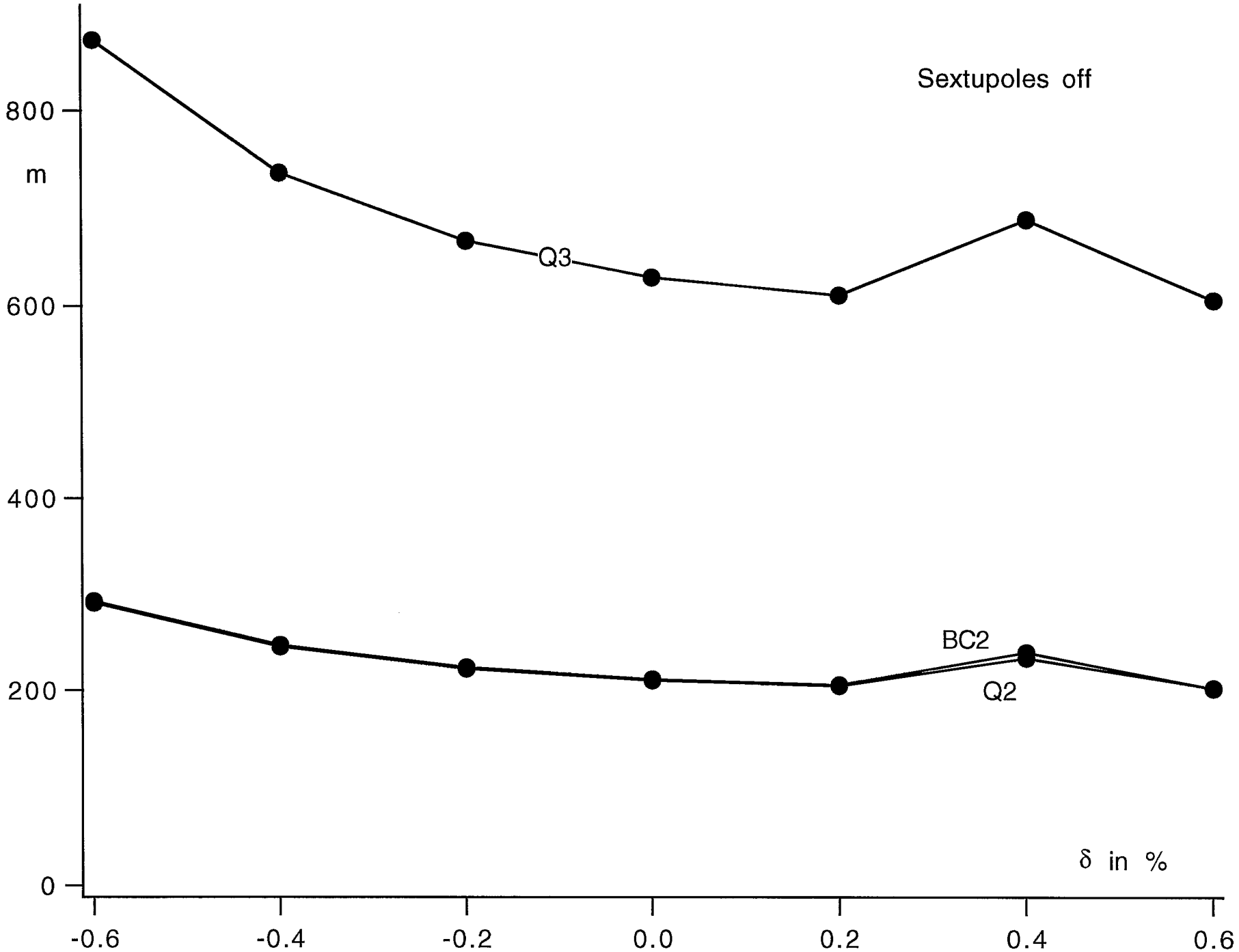

Fig. 11 β_V around aperture limitation vs. momentum error δ

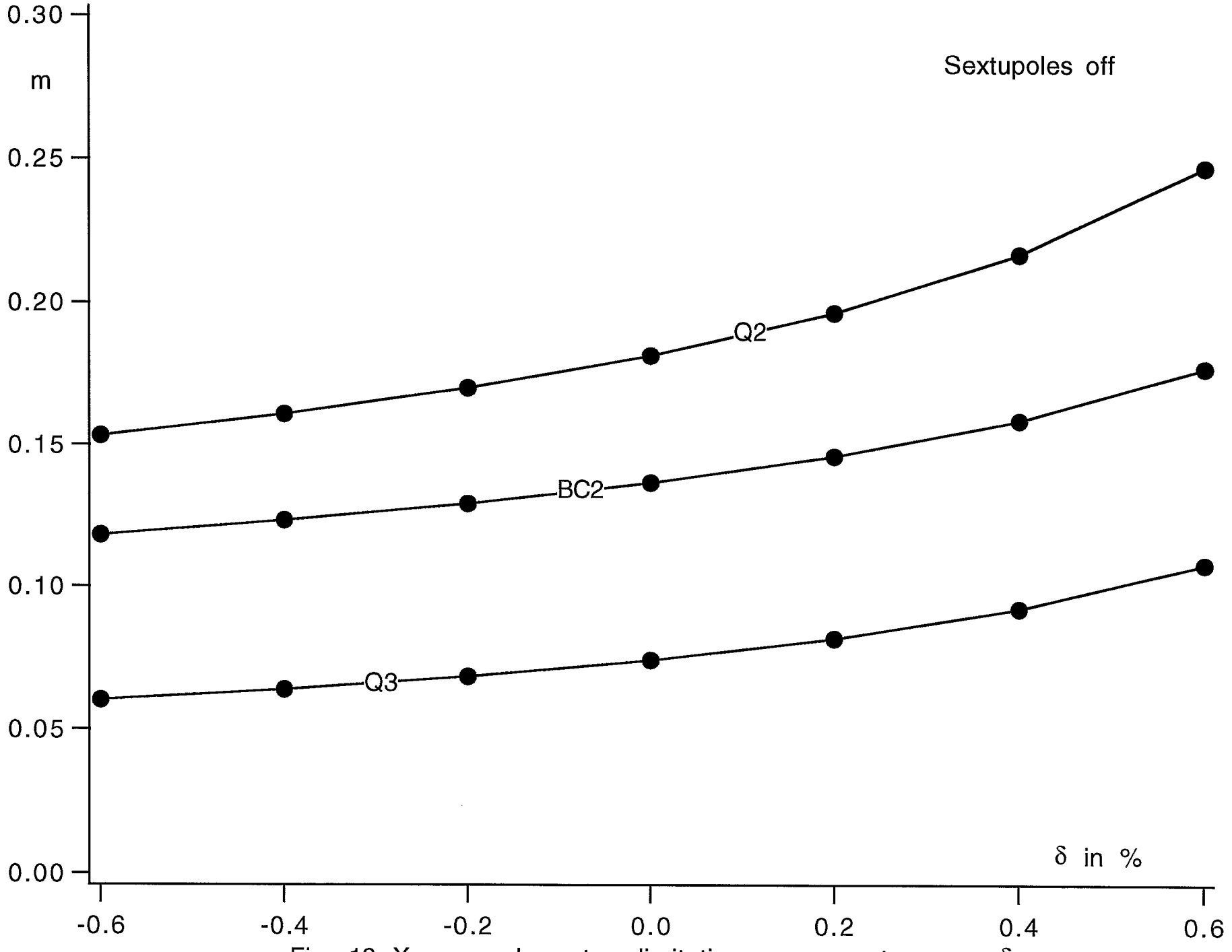

Fig. 12 X_p around aperture limitation vs. momentum error δ

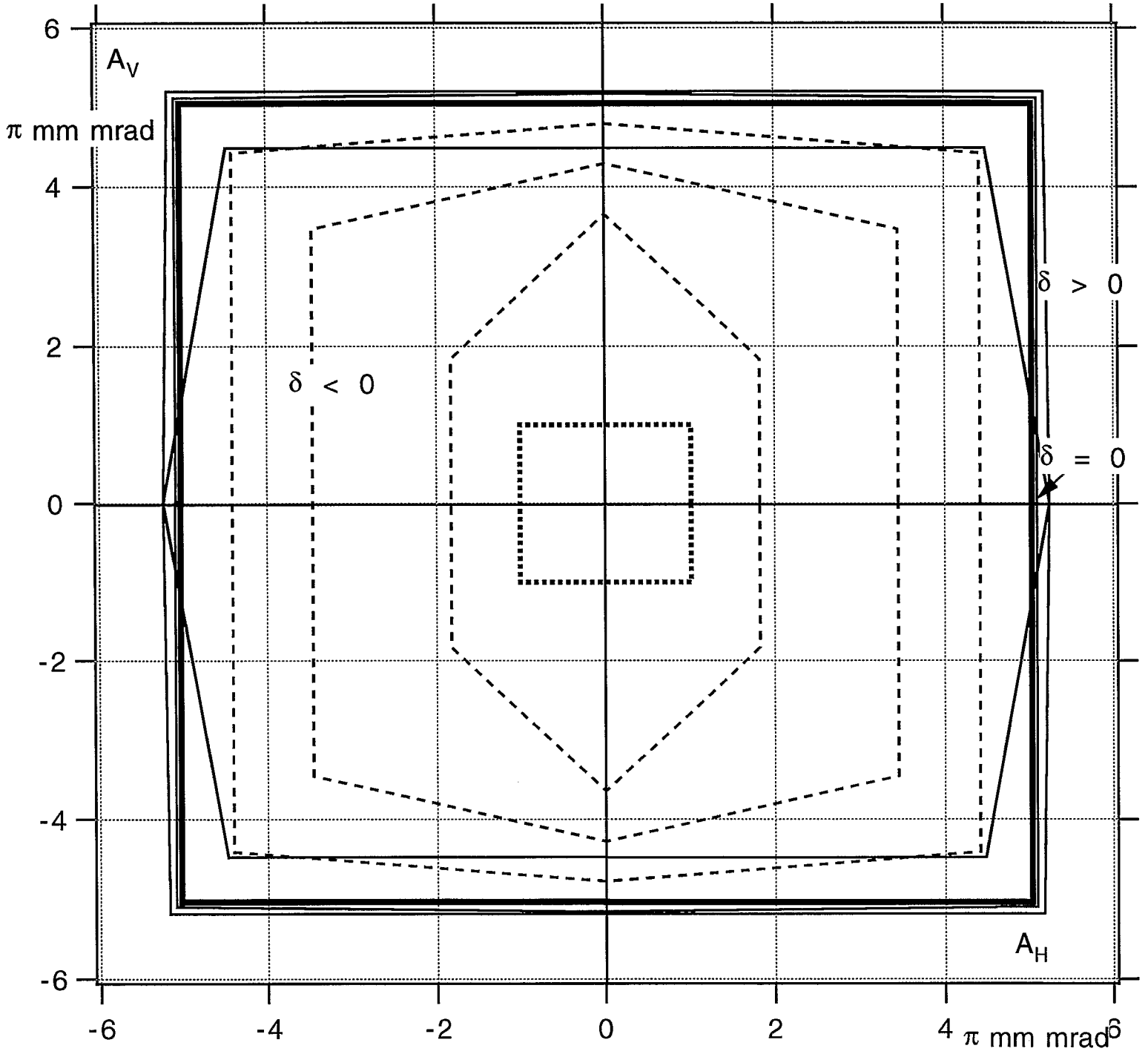

Fig. 13 Physical Acceptance with Sextupoles off

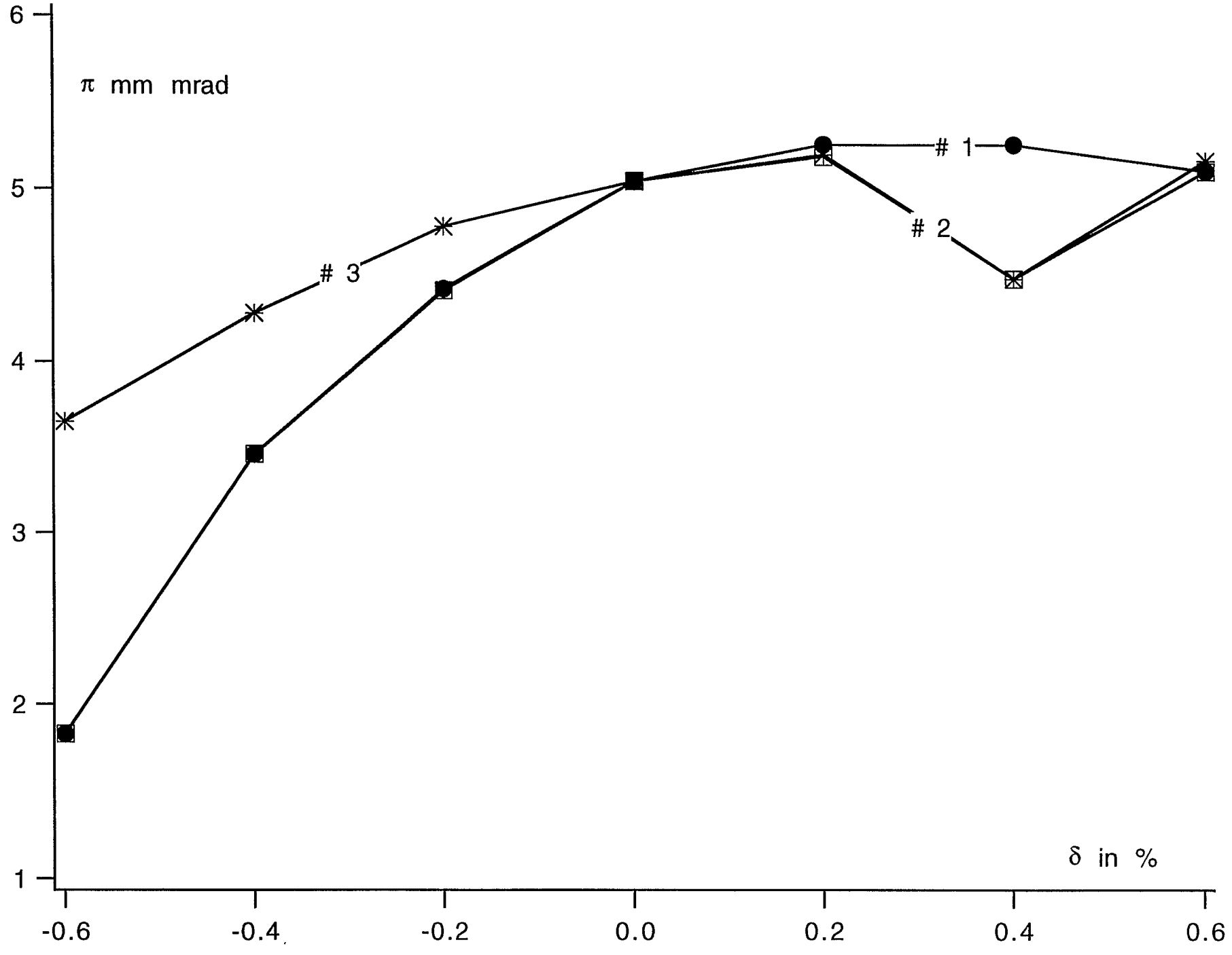

Fig. 14 Physical Acceptance with Sextupoles off

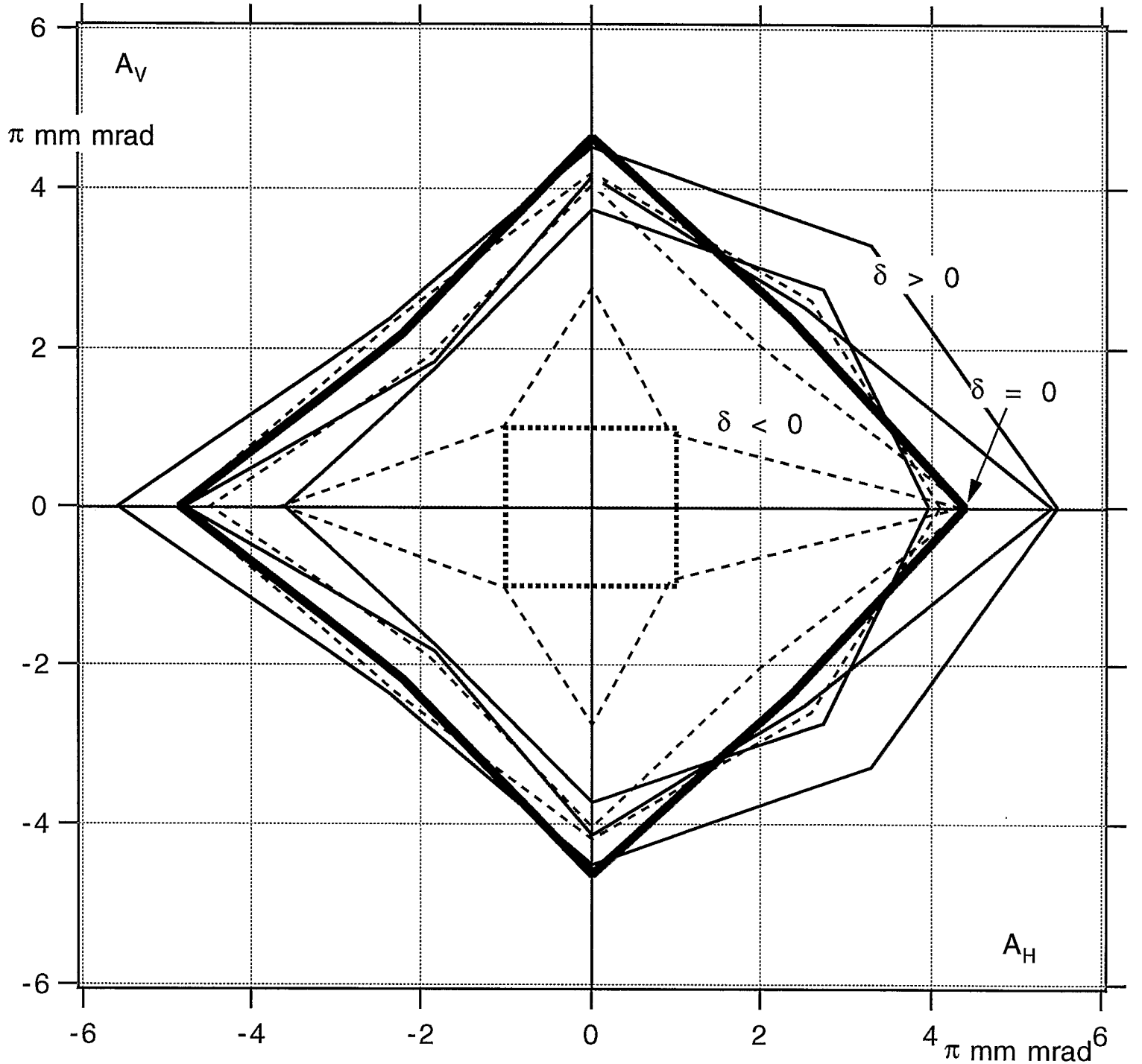

Fig. 15 Physical Acceptance with Sextupoles on

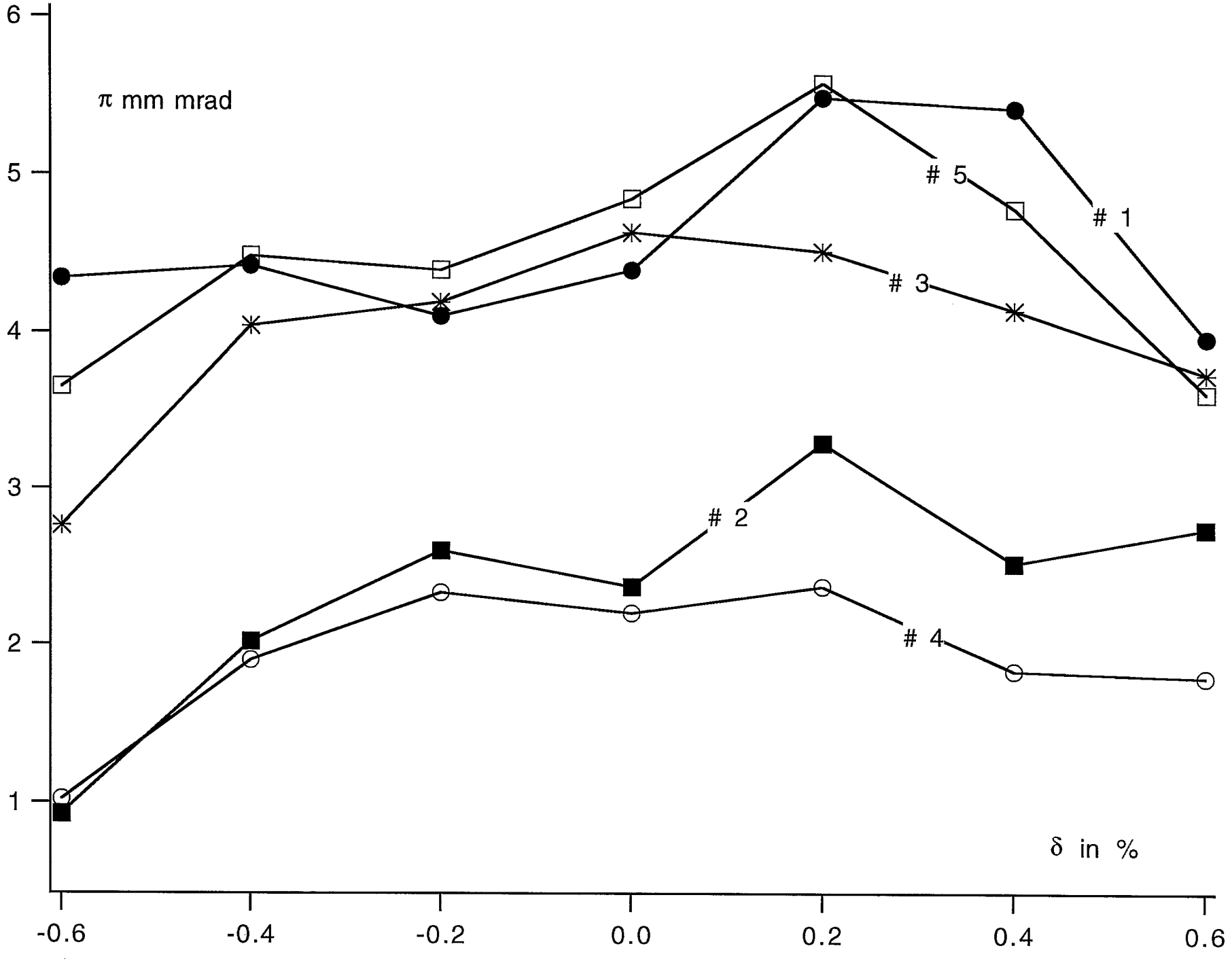

Fig. 16 Physical Acceptance with Sextupoles on

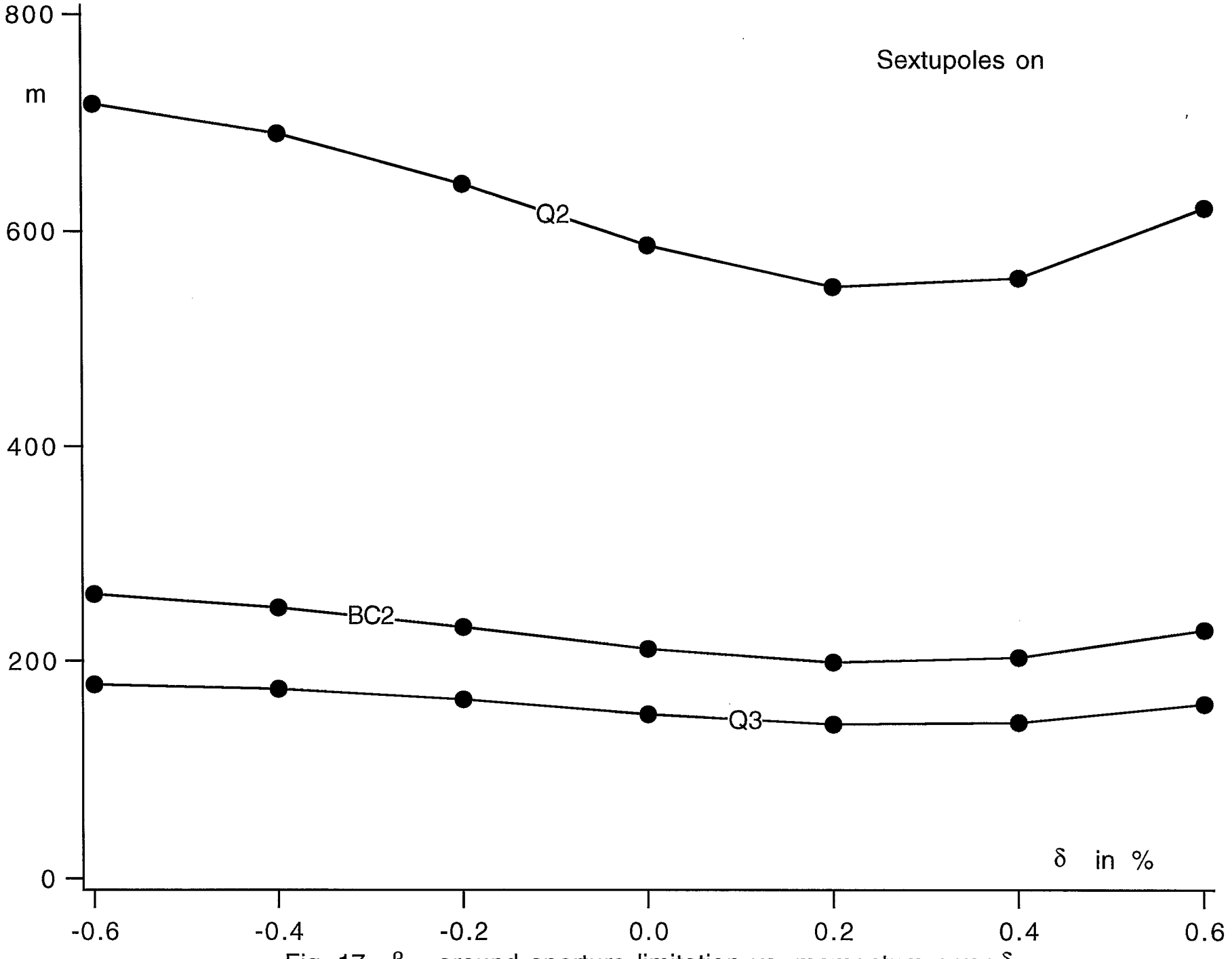

Fig. 17 β_H around aperture limitation vs. momentum error δ

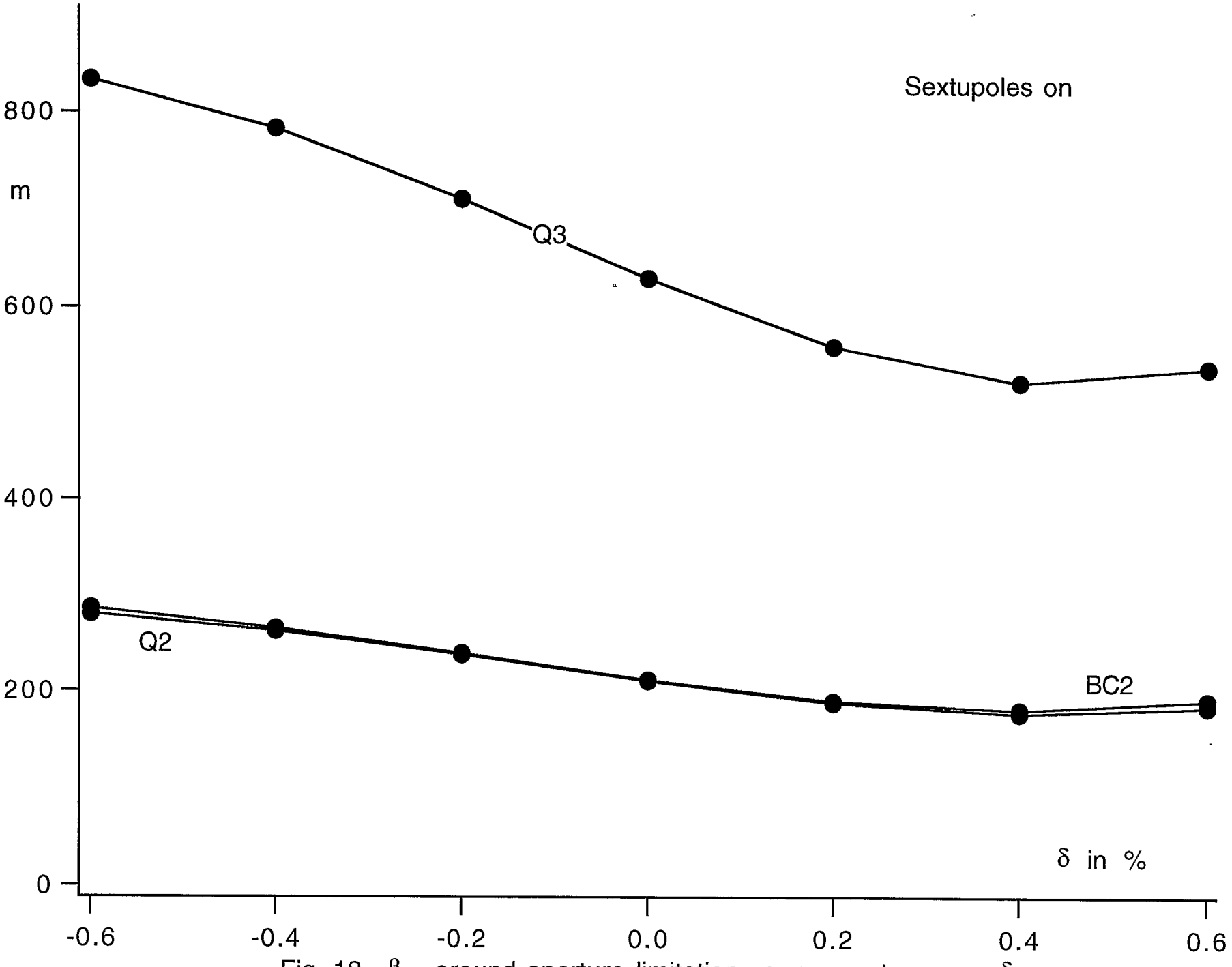

Fig. 18 β_V around aperture limitation vs. momentum error δ

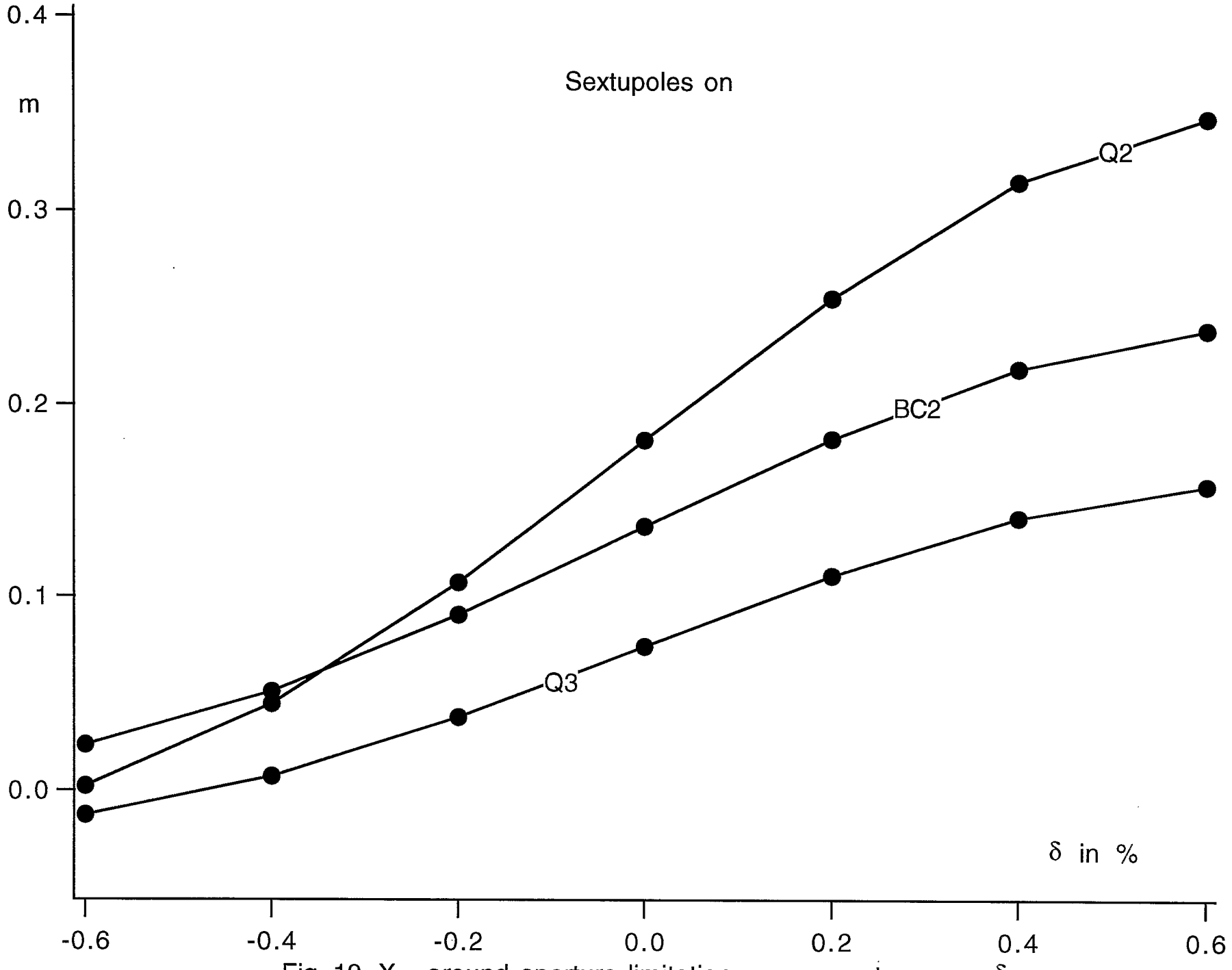

Fig. 19 X_p around aperture limitation vs. momentum error δ

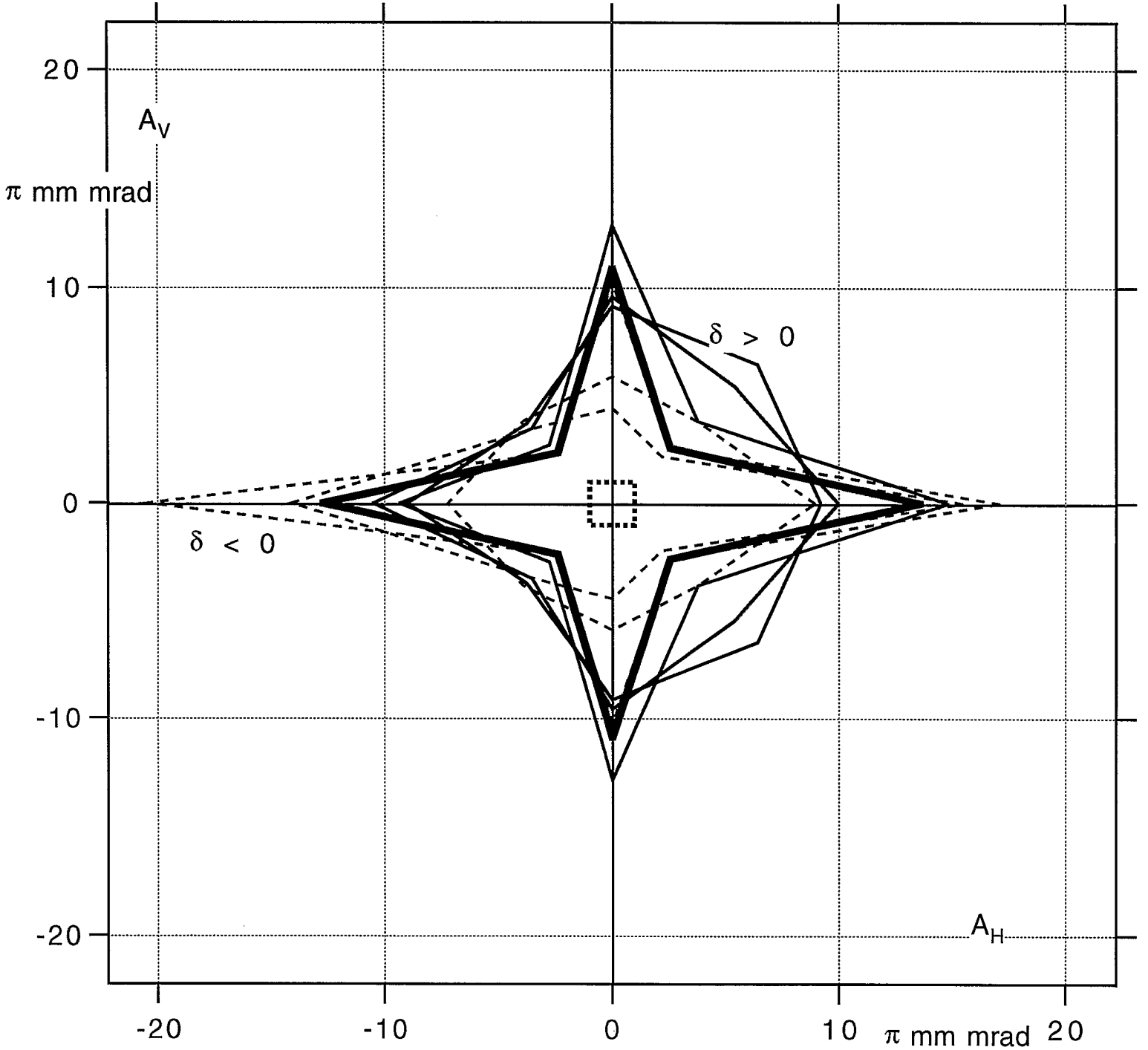

Fig. 20 Dynamic Aperture

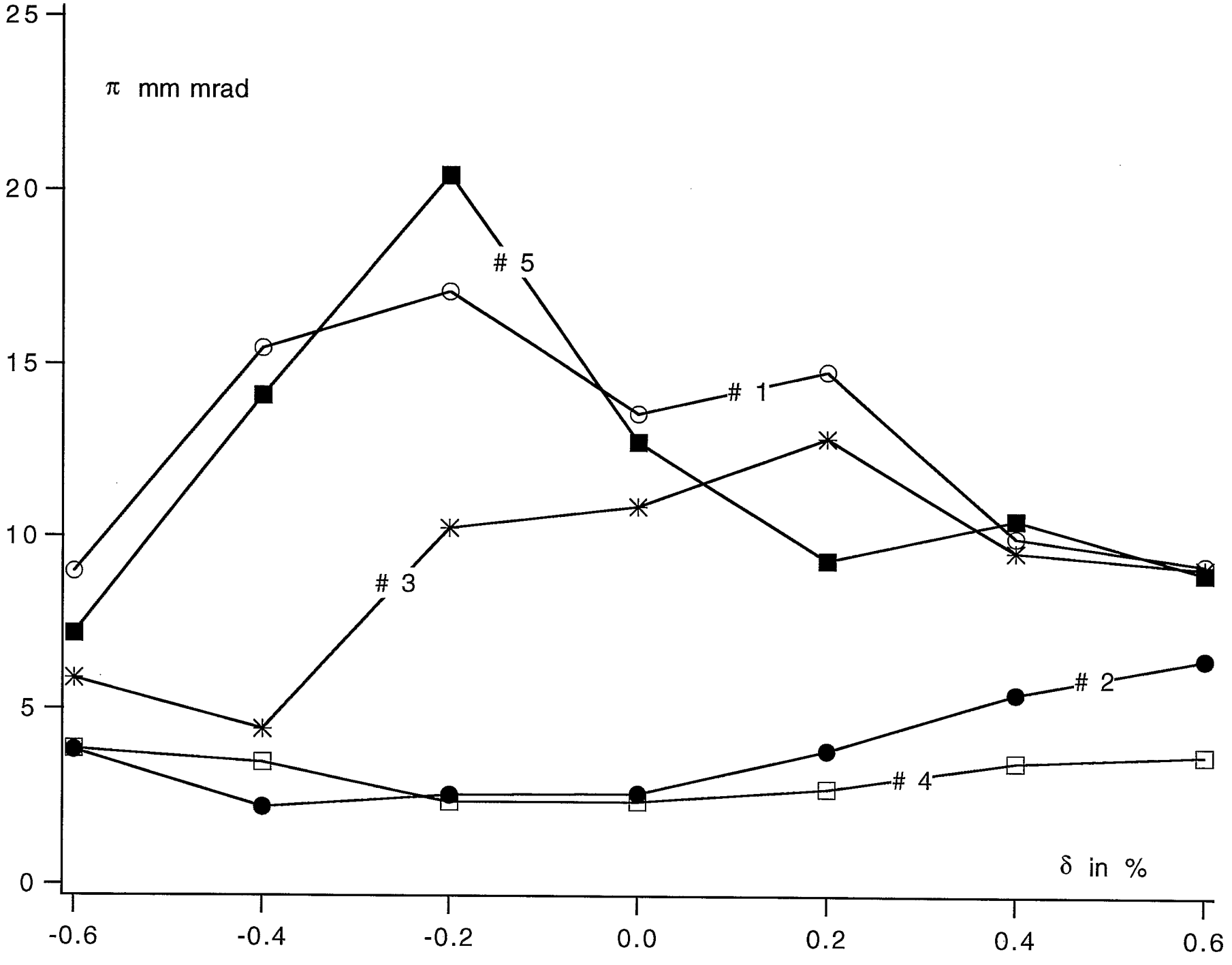

Fig. 21 Dynamic Aperture vs. Momentum Error δ

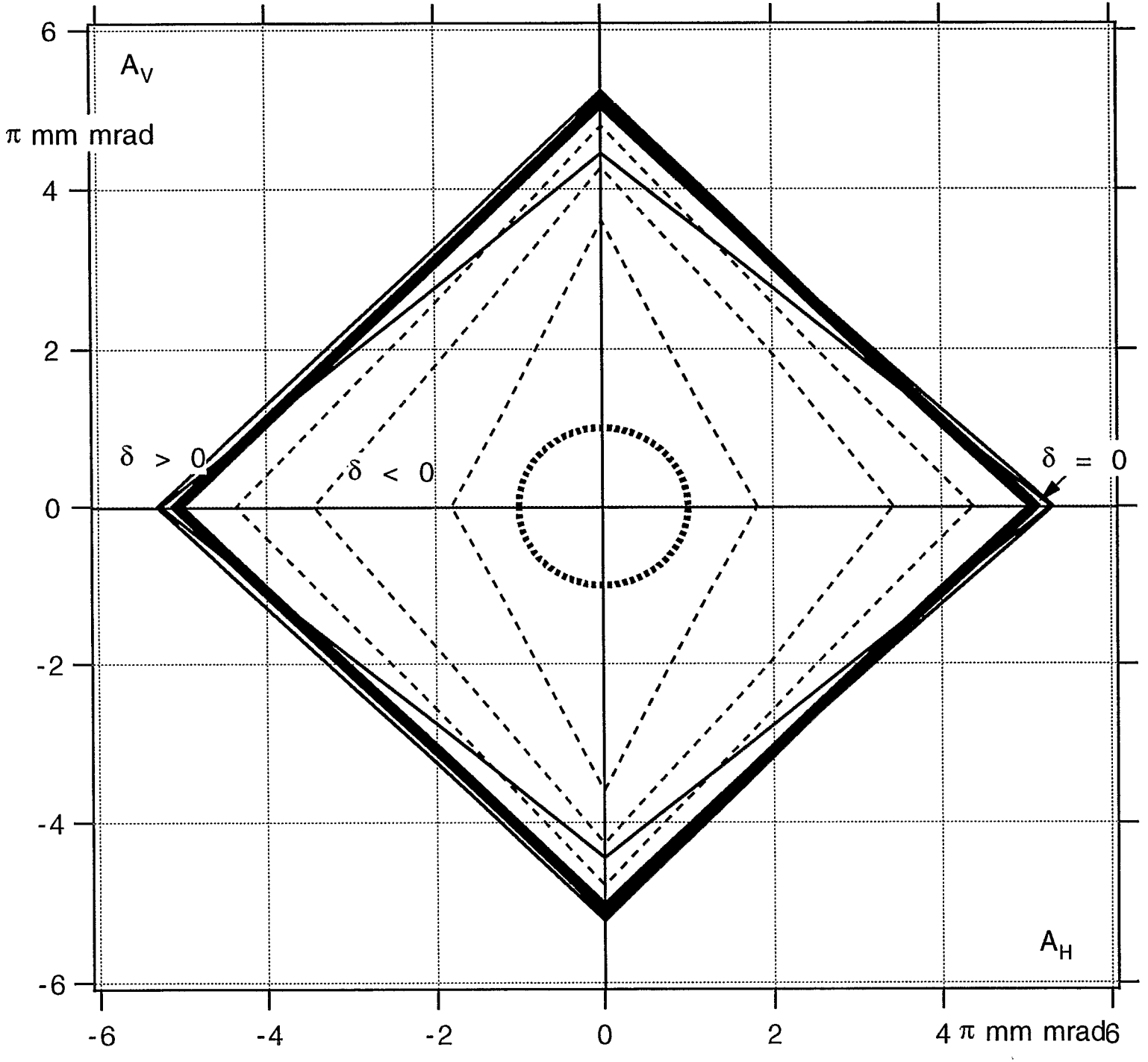

Fig. 22 Physical Acceptance with Sextupoles off

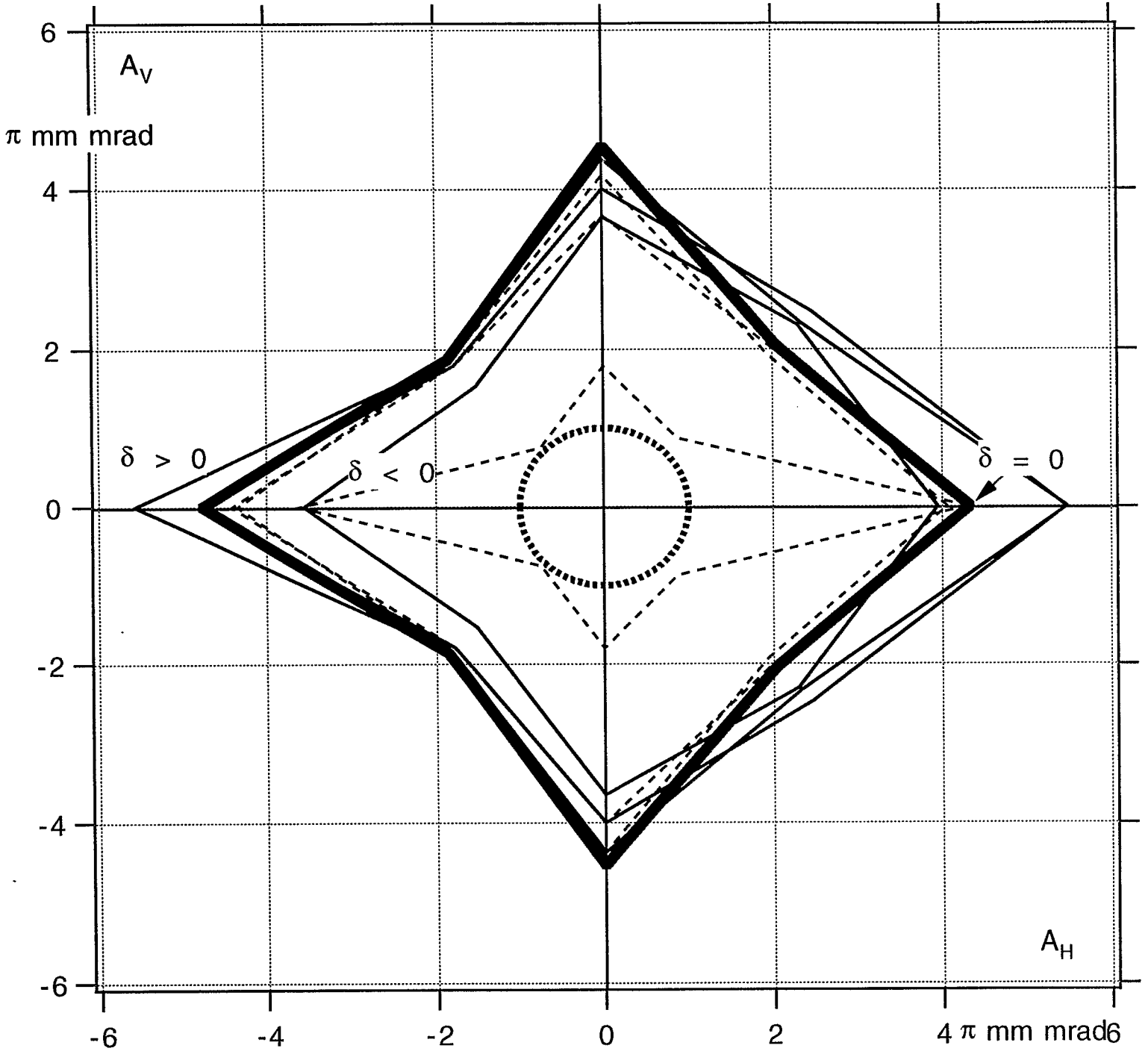

Fig. 23 Physical Acceptance with Sextupoles on

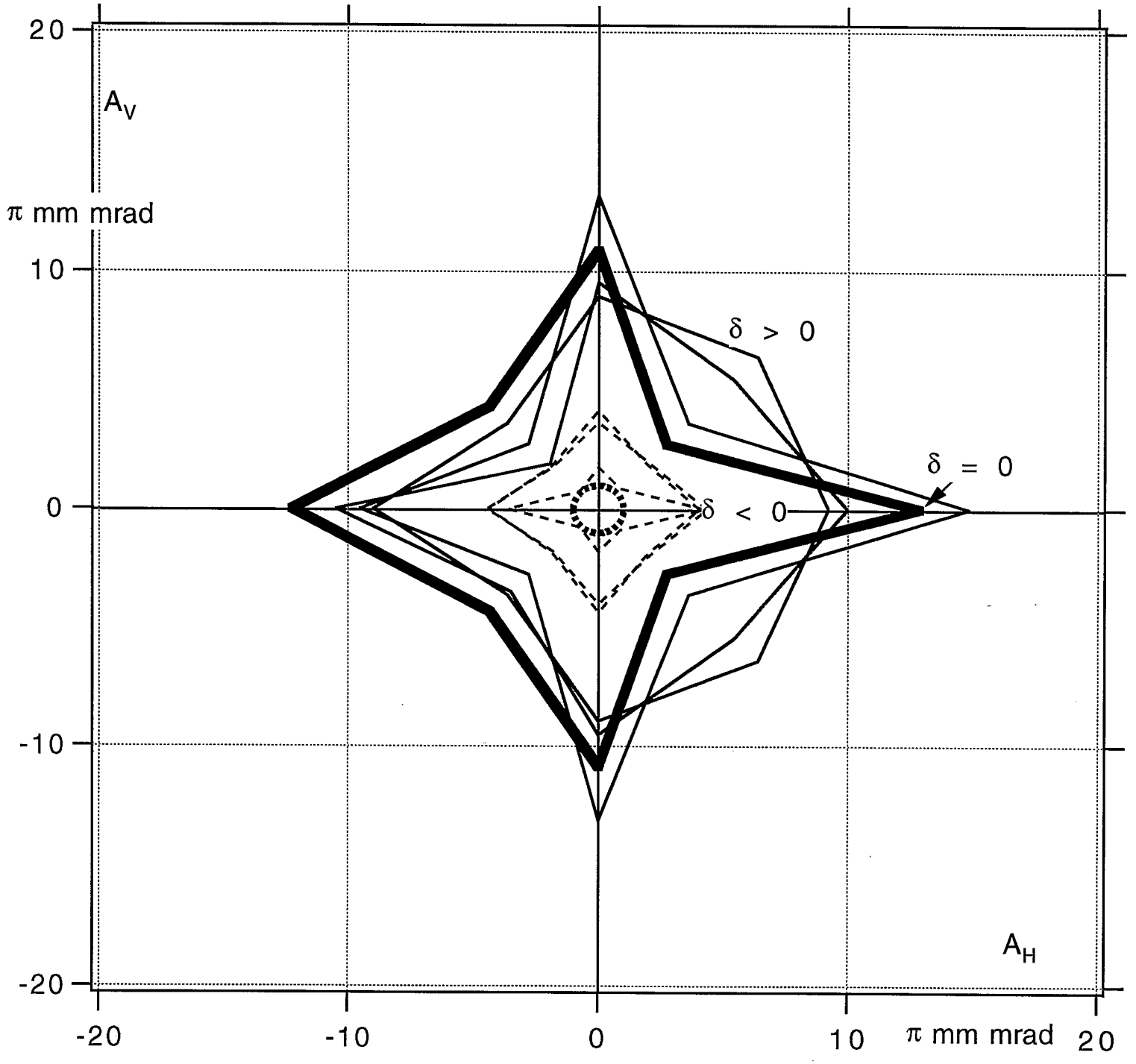

Fig. 24 Dynamic Aperture